

# Parametric Analysis of a Gasification-Based Cookstove as a Function of Biomass Density, Gasification Behavior, Airflow Ratio, and Design

Jonatan Gutiérrez, Edwin Lenin Chica, and Juan F. Pérez\*

Cite This: *ACS Omega* 2022, 7, 7481–7498

Read Online

ACCESS |



Metrics &amp; More

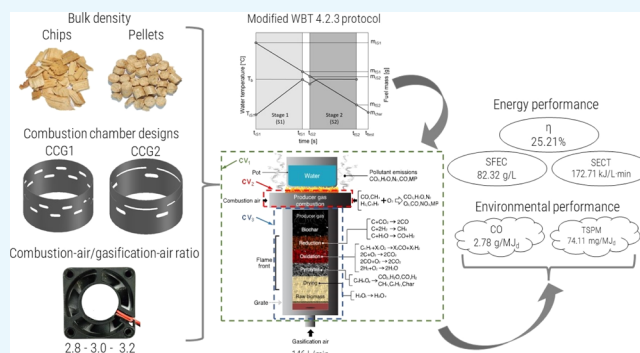


Article Recommendations



Supporting Information

**ABSTRACT:** The energy performance and emissions (carbon monoxide and total suspended particulate matter) of a biomass gasification-based cookstove under a modified water boiling test (WBT 4.2.3 protocol) were characterized here. The controllable process parameters analyzed were the biomass bulk density (pellets—WP and chips—WCH) and the combustion-air/gasification-air ratio (2.8, 3.0, and 3.2). Moreover, a design parameter of the cookstove was analyzed through two combustion chamber designs (combustion chambers 1 and 2). The cookstove was characterized in detail considering the complete cookstove (control volume 1), the combustion chamber (control volume 2), and the gasification process (control volume 3). The cookstove reached an average efficiency of 25.2% for pellets and 24.1% for chips. The best behavior for the cookstove was achieved when pellets were used, which is attributed to their higher bulk density and to the fact that during their gasification process, the biochar yield was 12% higher, while the biomass consumption decreased by 16% compared to the chips. The carbon monoxide specific emissions were 2.78 g/MJ<sub>d</sub> for pellets and 2.75 g/MJ<sub>d</sub> for chips. On average, the cookstove released total suspended particulate matter between 74.11 and 122.70 mg/MJ<sub>d</sub>. The cookstove low emissions are ascribed to the proper combustion air flow and the combustion chamber design, which favored the mixing between producer gas and combustion air.



## 1. INTRODUCTION

According to the World Health Organization (WHO), about 40% of the world population cook and heat their homes with open systems using biomass or carbon<sup>1</sup> due to the low cost and availability associated with these fuels.<sup>2</sup> In vulnerable communities of developing countries, these low-efficiency cookstoves are dominant while, simultaneously, affecting negatively the environment and quality of life and health of children, women, and the elderly, who usually spend more time at home and, consequently, are in contact with the stove combustion products.<sup>3,4</sup> Indoor air quality (IAQ) presents a risk factor for the health of people;<sup>5</sup> according to the WHO, every year more than 4 million people globally die due to diseases linked to pollution of indoor air in homes because of the use of solid fuels for cooking in traditional and inefficient systems.<sup>6</sup>

In Colombia, between 15 and 20% of the population use firewood as the main fuel source for cooking; that is, ~1.6 million homes use firewood daily to cook their food.<sup>7</sup> Cooking activities are usually performed in traditional three-stone fire (TSF) cookstoves,<sup>8</sup> which show low energy efficiencies (between 5 and 13%), higher fuel consumption, as well as higher pollutant emissions.<sup>9</sup> In Colombia, diseases such as ischemic heart disease, stroke, acute breathing infections, chronic obstructive pulmonary disease (COPD), and cataracts

are attributed to bad IAQ. In 2016, the total number of deaths in the country caused by the environmental load was of ~17,600, 13% of which was attributed to the ischemic heart disease and 17.6% resulted from COPD,<sup>10</sup> both diseases could be caused by exposition to emissions produced by traditional biomass cookstoves. Economical expenses to the country that can be attributed to these factors of environmental risk rose to (in US\$ millions) US\$ 83.3 for ischemic heart disease, US\$ 32.7 for stroke, US\$ 22 for lower-tract acute breathing infection, US\$ 7.0 for lung cancer, and US\$ 5.8 for COPD.<sup>10</sup>

Among the solution alternatives assessed by Colombia to reduce bad IAQ, the substitution of firewood in rural regions for liquid petroleum gas (LPG) can be named. However, this has not been possible due to the territorial expanse and the difficult access to isolated areas.<sup>11</sup> Additionally, costs by government subsidies for substituting firewood for LPG or electrical energy would rise to ~4170 US\$ million (~1.2% of

Received: September 15, 2021

Accepted: December 22, 2021

Published: February 24, 2022



Colombia GDP for 2019) in a program with a scope until 2050.<sup>12</sup> Thus, the biomass will continue being the main energy resource at isolated areas.<sup>13</sup> As a consequence, it is necessary to bring up different alternatives aimed at using in a more efficient way the biomass. In this regard, the development of efficient cookstoves with a lower biomass consumption and lower pollutant emissions (carbon monoxide—CO and particulate matter—PM) is highlighted. The Ministry of Environment and Sustainable Development has created the National Program of Efficient Stoves for Firewood Cooking, which aims at setting up a million of efficient stoves in Colombia by 2030.<sup>14</sup> Nevertheless, efficiency of the improved set up cookstoves are below 10–18%.<sup>8,15</sup> Therefore, minimum performance specifications have been defined for biomass-cooking systems by NTC 6358 standard of 2019.<sup>16</sup>

The development and implementation of advanced biomass cookstoves are explored and promoted, the cookstoves are based on gasification with a subsequent combustion of the producer gas. The adaptation of the gasification process at a lower scale (<20 kW<sub>th</sub>) for biomass cookstoves, whose efficiency might be  $\geq 25\%$ , is a useful application of sources of renewable energy to the everyday context.<sup>17</sup> The main product of the gasification-based or top-lit updraft (TLUD) cookstoves is the fuel gas,<sup>18</sup> whose thermochemical process is conducted similarly to the downdraft reactors.<sup>19</sup> This solid–gas conversion process can be thermodynamically characterized by the use of parameters such as the flame front velocity, biomass/air equivalence ratio, process temperature, composition, and heating value of the producer gas, as well as the gasification efficiency (cold gas efficiency), among others.<sup>20</sup> Generally, TLUD forced-draft stoves use fans to supply air for biomass gasification (gasification air or primary air), and producer gas combustion air (combustion air or secondary air). The aim is to generate a two-stage combustion process, reducing the pollutants released into the environment, due to a cleaner combustion when compared to TSF cookstoves.<sup>21–23</sup>

There are several international protocols for testing biomass cookstoves, which allow a comparison between different stove designs under different operation conditions.<sup>24–27</sup> Through the water boiling test (WBT), energy efficiency, fuel consumption, and specific pollutant emissions (CO and PM) could be determined in terms of operating parameters in the laboratory.<sup>28</sup> The efficiency of the gasification-based cookstoves varies with the design, air supply mode, and operating conditions, among other factors.<sup>29</sup> Considering the difference between natural and forced draft for TLUD cookstoves, Suresh et al.<sup>30</sup> reported efficiencies between 16 and 27% and from 30 to 35% for natural and forced draft cookstoves, respectively. Some TLUD cookstove designs have reached WBT efficiencies between 30 and 38%.<sup>31</sup> Besides, efficiencies around 42%, CO emissions of  $\sim 0.6$  g/MJ<sub>d</sub>, and PM of  $\sim 48$  mg/MJ<sub>d</sub> (stoves Tier 4) have been reported.<sup>32</sup> Sonarkar and Chaurasia<sup>26</sup> evaluated coconut shell, wood chips, and pellets as fuels in natural and forced draft cookstoves; the forced-draft cookstove, operating with wood pellets, reached the highest efficiency ( $\sim 43\%$ ).

Tryner et al.<sup>33</sup> found that the hydrogen (H<sub>2</sub>) content in the producer gas increased by 103% by using pellets concerning wood chips. This is attributed to higher temperatures and a longer residence time during pellet gasification, which favored a higher conversion of tars in light gases. Similar results were reported by Hanping et al.,<sup>34</sup> who noted that at a higher gasification temperature (800 °C), the gas energy content increased. With regard to the biomass moisture content,

Bhattacharya et al.<sup>35</sup> reported a reduction of  $\sim 43\%$  in the efficiency of a stove with an increase in the moisture content from 10 to 25%. Nevertheless, Van Zyl et al.<sup>36</sup> found that the specific emissions of CO and PM<sub>2.5</sub> increased by 84% and by 149%, respectively, when the biomass moisture is increased from 5 to 25%. However, a contrary trend was reported by Huangfu et al.,<sup>37</sup> where CO emissions decreased by  $\sim 39\%$  with the increase in the fuel moisture content.

Some improved biomass cookstoves can operate at Tier 3 or 4 levels, matching low pollutant emissions as the gas and liquid fuels cookstoves.<sup>9</sup> CO emissions of TLUD cookstoves are reduced due to the oxidation reaction with the secondary or combustion air.<sup>38</sup> The producer gas combustion in the combustion chamber of a TLUD cookstove must be in conditions close to the stoichiometry, aiming at increasing the efficiency and reducing pollutant emissions.<sup>39</sup> Mehta and Richards<sup>40</sup> found that combustion-air/gasification-air ratios higher than 4.0 do not have a significant effect on CO emissions, while a rise in the gasification-air flow from 24 to 33 L/min reduces CO emissions by  $\sim 50\%$ , with a combustion-air/gasification-air ratio of 2.0.

In turn, PM emissions from gasification-based cookstoves were reduced by 90% compared to TSF cookstoves.<sup>29,41</sup> Cookstoves operating at higher temperatures, such as cookstoves with compact designs, release a lower amount of PM.<sup>42,43</sup> Natural-draft cookstoves release  $\sim 473$  mg/L, while the forced-draft ones reach  $\sim 5.4$  mg/L.<sup>44</sup> Suresh et al.<sup>30</sup> found reductions between 21 and 57% of PM<sub>2.5</sub> emissions for TLUD forced-draft cookstoves compared to traditional cookstoves. Arora et al.<sup>45</sup> also reported a reduction between 39 and 47% of PM emissions by using a forced-draft cookstove with regard to a TSF cookstove. Carter et al.<sup>22</sup> informed that PM<sub>2.5</sub> emissions varied between 120 and 430 mg/MJ<sub>d</sub> for four Chinese cookstoves. Gupta et al.<sup>46</sup> reported PM<sub>2.5</sub> emissions from 83 to 290 mg/MJ<sub>d</sub> for a natural-draft cookstove. In turn, Kshirsagar and Kalamkar<sup>47</sup> developed a hybrid-draft thermally isolated cookstove with ceramic fiber, reaching PM<sub>2.5</sub> emissions of 34.67 mg/MJ<sub>d</sub>. It is highlighted that gasification-based cookstoves can reduce PM emissions by  $\sim 50\%$ , when compared to cookstoves of previous generations such as the rocket stove.<sup>48</sup> Other works have evaluated the total suspended particulate matter,<sup>25,49,50</sup> which corresponds to PM in the entire range of particle size released by the gasification cookstoves. Kaur-Sidhu et al.<sup>51</sup> reported total suspended particulate matter emissions in the range comprised from 0.86 to 1.67 mg/m<sup>3</sup> in improved cookstoves operating with three types of biomass, compared with 0.31 and 0.57 mg/m<sup>3</sup> for the LPG and kerosene, respectively.

In this work, the performance of a gasification-based cookstove is assessed in terms of the following: (a) process controllable parameters (e.g., biomass bulk density and combustion-air/gasification-air ratios), (b) gasification condition of two types of biomass, including chips and pellets, and (c) design parameters of the cookstove through two combustion chambers. Furthermore, the gasification-based biomass cookstove is divided and characterized considering three control volumes (the cookstove, the combustion chamber, and the gasification process). The gasification process of biomass in a fixed bed, whose thermochemical solid–gas conversion process is one of the main steps in the TLUD cookstove, is characterized and its assessment in this type of cookstoves is scarce.<sup>33</sup> According to the literature reported, these parameters have not been studied in a coupled

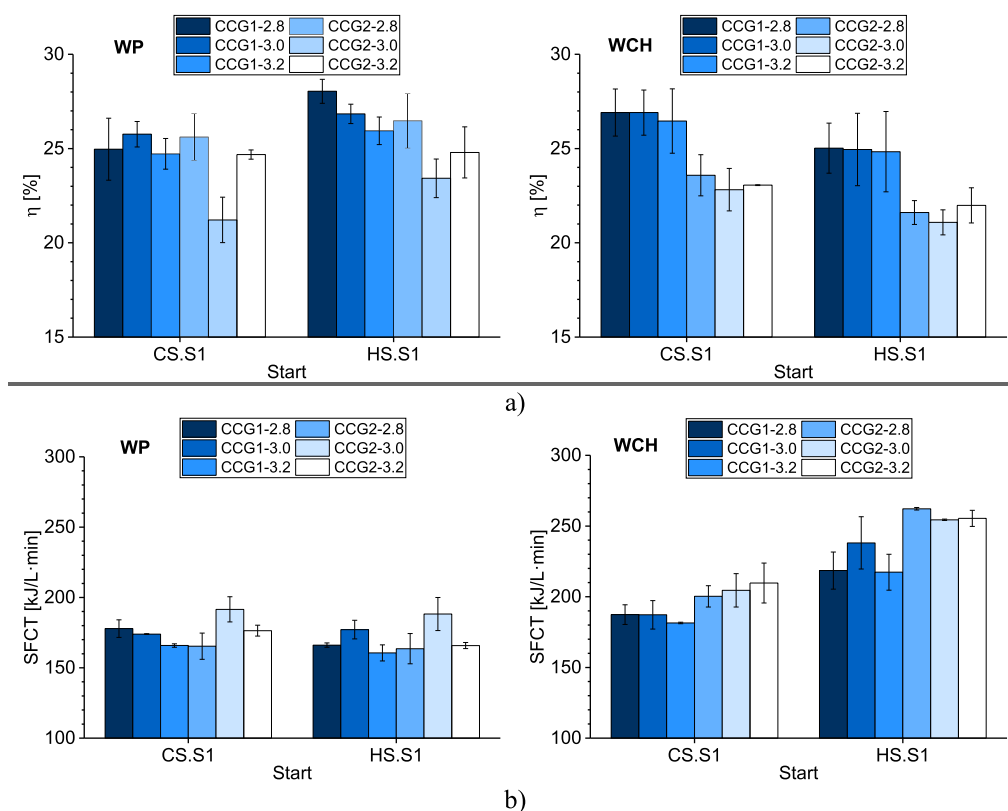


**Figure 1.** Energy parameters of the gasification-based cookstove in WBT-S1 under cold and hot starts [cold start—stage 1 (CS.S1) and hot start—stage 1 (HS.S1)]. (a) Efficiency— $\eta$  (%), and (b) specific energy consumption per unit time—SFCT (kJ/L·min).

method, which supposes a contribution to the phenomenological understanding and to the development of advanced biomass cookstoves.<sup>30</sup>

## 2. RESULTS AND DISCUSSION

### 2.1. Control Volume 1 (CV<sub>1</sub>): Gasification-Based Cookstove.

The gasification-based cookstove is characterized both energetically and environmentally under a modified WBT 4.2.3 protocol, through the analysis of the control volume 1. The study was carried out in two sections: (1) assessment of the experimental factors and their levels during stage 1 (S1) of the modified WBT 4.2.3 protocol (WBT-S1) with both starting methods, cold start (CS) and hot start—HS (cold start stage 1—CS.S1, and hot start stage 1—HS.S1),<sup>47,52</sup> and (2) assessment of the factors and their levels thoroughly following the modified WBT 4.2.3 protocol (CS.S1, cold start stage 2—CS.S2, HS.S1, and hot start stage 2—HS.S2) for determining the specific emissions of total suspended particle matter with pellets.

#### 2.1.1. Biomass Density, Combustion-Air/Gasification-Air (CA/GA) Ratio, and Combustion Chamber of the Producer Gas (CCG) under WBT-S1. 2.1.1.1. Energy Performance.

Figure 1 shows the energy parameters such as thermal efficiency ( $\eta$ , %), and the specific energy consumption per unit time (SFCT, kJ/L min) of the gasification-based cookstove under cold start—stage 1 and hot start—stage 1, as a function of the experimental factors and their levels: biomass bulk density (2 levels, pellets—560 kg/m<sup>3</sup> and chips—151 kg/m<sup>3</sup>), combustion-air/gasification-air ratio (3 levels, 2.8, 3.0, and 3.2), and combustion chamber design (2 levels, combustion chambers 1 and 2). The legends of the result figures show the response variables parameterized with

the following code combustion chamber—combustion-air/gasification-air, indicating the combustion chamber design and the combustion air-gasification air ratio linked to each result. In Figure 2, the statistical significance through the Pareto chart

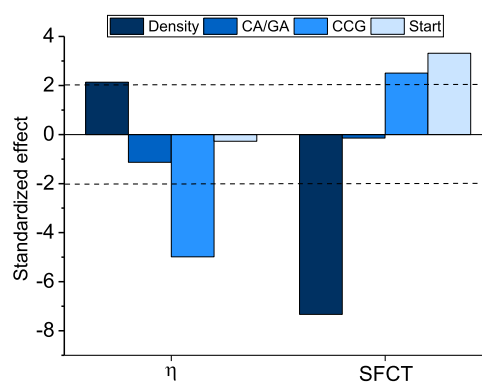


**Figure 2.** Pareto chart: effect of the biomass density, combustion-air/gasification-air (CA/GA) ratio, combustion chamber (CCG) design, and start type on the energy parameters of the gasification-based cookstove under cold start—stage 1 and hot start—stage 1.

with a confidence level of 95% for each response variable analyzed through this experiment design (Section S3.1, Supporting Information) is depicted.

**Thermal Efficiency ( $\eta$ , %):** According to the Analysis of Variance (ANOVA), the biomass density has a statistically significant effect on the efficiency (Figure 2). The average efficiency with pellets was 25.21, ~5% higher compared to the average efficiency reached with chips, whose value was 24.1% (Figure 1a). The higher efficiency reached with pellets is

ascribed to two aspects. First, the biochar mass yield— $Y_{\text{biochar}}$  (eq S8), which was 12% higher for the pellets in comparison to the chips, with average values of 12.12 and 10.82%, respectively. Second, the biomass consumption rate ( $\dot{m}_{\text{bms}}$ , kg/h·m<sup>2</sup>), which was ~16% higher for the chips. The higher biochar mass yield and lower biomass consumption rate of the pellets were reached due to their bulk density, which is 3.7 higher than that of the chips,<sup>53,54</sup> as it is explained in the control volume 3 (Section 2.3). As the biomass-packing factor increases, the radiative heat transfer penetration in the solid phase decreases,<sup>55</sup> thus generating a lower biomass consumption and a higher biochar yield for the pellets.<sup>19,56</sup> Therefore, the energy supplied by the biomass to boil the water decreases (eq S11), and consequently, the efficiency increases (eq S12). It is worth noting that the efficiency of the TLUD cookstove analyzed in this study was 80 and 72% superior with pellets and chips, respectively, compared to TSF cookstoves with thermal efficiencies of ~14%.<sup>46,57</sup> Besides, by contrasting the efficiency of the TLUD cookstove with other improved cookstoves, it is concluded that the thermal efficiencies reached herein are comparable with gasification cookstoves whose efficiencies ranged between 23 and 28.8%.<sup>46,58</sup>

The combustion-air/gasification-air ratio does not have a statistically significant effect on the efficiency (Figure 2). This is attributed to the fact that the conditions of the combustion-air flow (408.8, 438.0, and 467.2 L/min for the combustion-air/gasification-air ratios 2.8, 3.0, and 3.2, respectively) are similar. In Supporting Information S4, CFD simulation of the combustion air through the combustion chambers is shown. As a consequence, the energy and the environmental parameters of the gasification-based cookstove do not vary significantly as a function of the combustion-air/gasification-air factor with the ratios assessed in this work. It is highlighted that the combustion air flow velocities are adequate because the combustion flame was not extinguished during the producer gas oxidation. Caubel et al.<sup>52</sup> stated that a higher velocity of combustion air injection (secondary air) improves the performance of the cookstove; however, an excessive combustion air flow might cause the flame extinction.

The design of the combustion chamber of the producer gas was the factor with the highest effect on efficiency (Figure 2). The efficiency of the cookstove working with pellets and combustion chamber 1 in the cold start—stage 1 was 25.15%, compared to 23.84% for combustion chamber 2 (Figure 1a). A similar behavior was found comparing combustion chamber 1 (26.94%) and combustion chamber 2 (24.90%) in the hot start—stage 1 with pellets, originating an efficiency of 8.2% higher for combustion chamber 1. For the chips, a similar trend was observed for efficiency, although the differences are higher between the combustion chambers (Figure 1a). For the cold start—stage 1, the efficiency of the cookstove was 26.76% with combustion chamber 1, while combustion chamber 2 reached 23.15%. This indicates that the combustion chamber 1 reached an efficiency of 16% higher. In the hot start—stage 1 with chips, the efficiency values were 24.93 and 21.56% for the combustion chambers 1 and 2, respectively. This means an efficiency of 15.6% higher for the combustion chamber 1. The highest efficiency reached for the TLUD cookstove with the combustion chamber 1 is attributed to its higher levels of turbulence (see Section 2.2). The higher turbulence level at the exit of the combustion air in the combustion chamber 1 led to an increase in the residence time of the producer gas in the

combustion zone, while oxygen is supplied directly to the rich-fuel regions. Thereby, a more complete oxidation of the producer gas is promoted, and consequently, the efficiency increases.<sup>52</sup>

In this particular case, the type of start did not have a statistically significant effect on the efficiency (Figure 2). The efficiency with pellets under cold start—stage 1 was 24.49% and under the hot start—stage 1 was 25.92% (Figure 1a), indicating an increase of 6% moving from cold start—stage 1 to hot start—stage 1. In contrast, for the chips, the efficiency decreased by 7% by going from 24.96% in cold start—stage 1 to 23.25% in hot start—stage 1 (Figure 1a). The higher value of efficiency reached with the pellets in hot start—stage 1 is related to the gasification process. The gasification of the pellets under hot start promotes the production of fuel gaseous species (CO and methane—CH<sub>4</sub>) for the higher biomass burning velocity ( $V_b$ , mm/min) and fuel/air equivalence ratio ( $F_{\text{rg}}$ ), see analysis of the control volume 3 (Section 2.3). For the pellets under the hot start—stage 1, the heating value of the producer gas (LHV<sub>pg</sub>) and the biomass consumption rate increased by 17 and 18%, respectively. While, for the chips under hot start—stage 1, the heating value of the producer gas increased by ~6%, but the biomass consumption rate increased by ~22%, which led to a lower efficiency in the hot start—stage 1.

*Specific Energy Consumption Per Unit Time (SFCT, kJ/L·min)*: the biomass density statistically affects the specific energy consumption per unit time (Figure 2). The average specific energy consumption per unit time value for pellets was 172.71 kJ/L·min, while the cookstove fed with chips reached 218.04 kJ/L·min (Figure 1b). This means a specific energy consumption per unit time 21% higher for the chips. This result is a consequence of a lower specific energy consumption (Section S5, Supporting Information) and a higher duration time of the test ( $t_{\text{test}}$ , s) reached for the pellets (eq S14). The difference in the test time between the pellets and the chips was ~18%, with values of 544 and 462 s, respectively. This result, as it is analyzed in Section 2.3, is attributed to a biomass/air equivalence ratio ( $F_{\text{rg}}$ ) ~22% higher for the chips compared to the pellets. The high biomass/air equivalence ratio of the chips is due to a higher reaction velocity and a higher biomass consumption rate. Furthermore, the specific energy consumption per unit time is lower for biomasses with a higher ash content due to a lower oxidant-fuel contact.<sup>55</sup> In this work, the ash content of the pellets is ~4 times higher than that of the chips (Table 1). The specific energy consumption per unit time of the gasification-based cookstove characterized in this work is similar to what was reported by Osei et al., with values ~170 kJ/L·min.<sup>31</sup>

The design of the combustion chambers has a significant effect on specific energy consumption per unit time (Figure 2). The cookstove specific energy consumption per unit time, fed with pellets under cold start—stage 1, reached values of 172.56 kJ/L·min with combustion chamber 1 and 177.78 kJ/L·min with combustion chamber 2 (Figure 1b), leading to a specific energy consumption per unit time 3% higher with combustion chamber 2. Under the hot start—stage 1 with pellets, the cookstove reached a specific energy consumption per unit time of 168.96 kJ/L·min with combustion chamber 1 and 172.55 kJ/L·min with combustion chamber 2. The specific energy consumption per unit time was 3% higher for combustion chamber 2. Additionally, the specific energy consumption per unit time of the TLUD cookstove with chips under cold

**Table 1. Physicochemical and Energy Properties of the Biomass Samples (Pellets and Chips)**

property	standard	biomasses	
		pellets	chips
Ultimate Analysis d.a.f. (wt %)			
C	ASTM D5378-08	46.83	47.38
H	ASTM D5378-08	5.67	6.08
O	by difference	47.48	46.38
N	ASTM D5378-08	0.02	0.16
Proximate Analysis d.b. (wt %)			
volatile material	ASTM D5142-04	84.64	83.83
fixed carbon	by difference	14.09	15.85
ash content	ASTM D5142-04	1.27	0.32
moisture content (wt %)	ASTM D5142-04	7.91	11.12
Physical Properties			
bulk density (kg/m <sup>3</sup> )		559.97	151.29
particle density (kg/m <sup>3</sup> )		1153.62	416.24
packing factor (-)		0.48	0.36
particle sphericity (-)		0.87	0.7
Energy Properties			
HHV (MJ/kg)	ASTM E144-14	20.36	18.34
LHV (MJ/kg)	calculated	19.03	16.85

start—stage 1 was 185.33 kJ/L·min with combustion chamber 1 and 204.84 kJ/L·min with combustion chamber 2, which means that the specific energy consumption per unit time is 10% higher with combustion chamber 2. While for chips under the hot start—stage 1, specific energy consumption per unit time was 224.64 kJ/L·min with combustion chamber 1 and 257.33 kJ/L·min with combustion chamber 2 (13% higher with combustion chamber 2). This behavior is due to the less favorable combustion conditions with combustion chamber 2 because of the geometric configuration and dimensions of the grooves,<sup>52</sup> as it was analyzed in the specific energy consumption (Section S5, Supporting Information).

The start type has a statistically significant effect on the specific energy consumption per unit time (Figure 2). The pellets reached a specific energy consumption per unit time of 175.17 kJ/L·min under the cold start—stage 1 and 170.25 kJ/L·min under hot start—stage 1 (Figure 1b). This results in a decrease of 3% in the specific energy consumption per unit time for the hot start—stage 1. Concerning the chips, the specific energy consumption per unit time increased by 19% from cold start—stage 1 to hot start—stage 1, with values of 195.08 and 240.99 kJ/L·min, respectively. With the cookstove

fed with pellets, the time elapsed during the test from cold start—stage 1 (550 s) to hot start—stage 1 (538 s) decreased by 2%. This caused a mild change in the specific energy consumption per unit time when going from cold start—stage 1 to hot start—stage 1 (3%). In the cold start—stage 1, a fraction of the biomass energy is used for heating the metallic body of the cookstove. Meanwhile, in the hot start—stage 1, the heat transfer to the reactor wall decreases, favoring that the specific energy consumption per unit time decreases in the hot start—stage 1.<sup>46</sup> The increase in the specific energy consumption per unit time found for the chips under hot start—stage 1 is a consequence of the reduction in the test time (~15%), which ranged from 497 s in cold start—stage 1 to 434 s under hot start—stage 1. The test time reduction is due to the higher biomass consumption rate for the chips because of their lower bulk density and by the TLUD cookstove preheating.

**2.1.1.2. Specific Emissions of Carbon Monoxide and Total Suspended Particulate Matter. Carbon Monoxide Specific Emissions (g/MJ<sub>d</sub>):** Figure 3 shows the carbon monoxide specific emissions (EF<sub>CO</sub>) of the gasification-based cookstove as a function of the experimental factors (Section S3.1, Supporting Information). In turn, in Figure 4, the ANOVA results through the Pareto chart for the specific emissions of CO with a 95% confidence level are represented.

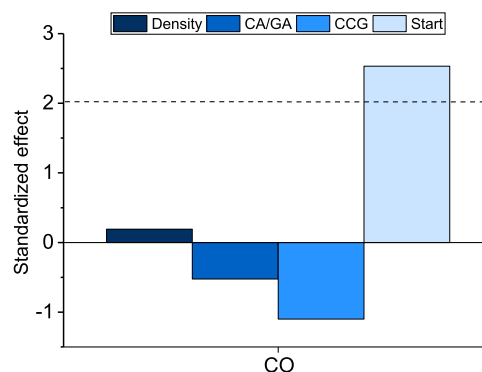


**Figure 4.** Pareto chart: effect of the biomass density, combustion-air/gasification-air ratio (CA/GA), combustion chamber (CCG) design, and start type (cold and hot) on the specific emissions of CO—EF<sub>CO</sub> (g/MJ<sub>d</sub>) of the gasification-based cookstove.

The factor that affects the specific emissions of CO in a statistically significant mode is the type of start in the WBT

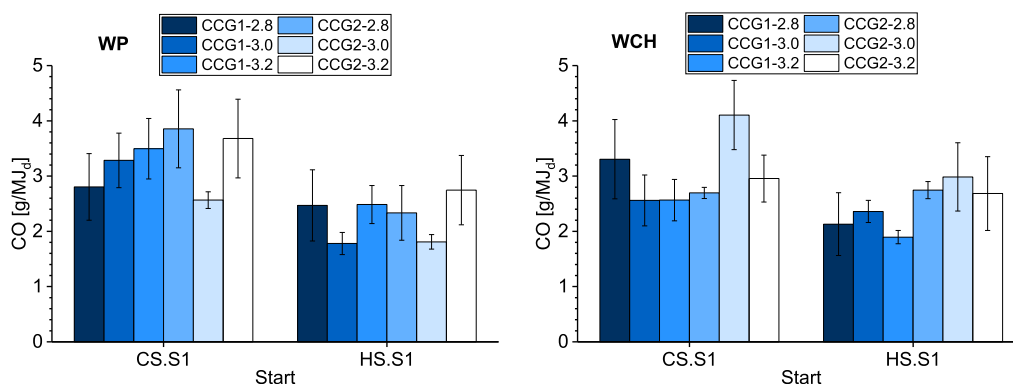


**Figure 3.** Specific emissions of CO—EF<sub>CO</sub> (g/MJ<sub>d</sub>) of the gasification-based cookstove in the stage 1 of cold and hot starts [cold start—stage 1 (CS.S1) and hot start—stage 1 (HS.S1)].

protocol, while the biomass density, the combustion-air/gasification-air ratio, and the combustion chamber design do not statistically affect the CO emissions (Figure 4). Considering the biomass density, the average specific emissions of CO of the TLUD cookstove with pellets was 2.78 g/MJ<sub>d</sub>, while the chips reached an average value of 2.75 g/MJ<sub>d</sub> (Figure 3). The slight variation of the specific emissions of CO between pellets and chips is because both biomasses correspond to the same forest species, and thus, their chemical composition of these fuels is similar. Therefore, the specific emissions of CO was similar.<sup>54</sup> Nevertheless, the mild difference of the specific emissions of CO between both biomasses might be attributed to the fact that fuels with high heating value tend to produce higher CO emissions.<sup>46</sup> Here, HHV of the pellets is 11% higher than that of the chips (Table 1). Compared to the TSF cookstoves, which use wood as fuel, and whose specific emissions of CO was 15.7 g/MJ<sub>d</sub>,<sup>59,60</sup> the CO emissions for the gasification-based cookstove decrease by ~82%. Besides, with respect to other gasification-based cookstoves, the results concerning the specific emissions of CO are consistent. Gupta et al.<sup>46</sup> found CO emissions of 3.62 g/MJ<sub>d</sub> for a gasification cookstove fed with wood. Osei et al.<sup>31</sup> reported a CO emission factor of 55.77 g/kg, while the TLUD cookstove in this work reached a CO emission factor of 52.90 and 46.34 g/kg for pellets and chips, respectively.

The combustion-air/gasification-air ratio does not have a statistically significant effect on the specific emissions of CO due to similar combustion air flow conditions when working under the combustion-air/gasification-air ratios of 2.8, 3.0, and 3.2. This finding is similar to the one found by Tryner et al.,<sup>33</sup> who reported a minimum in CO emissions for flow ratios of secondary air/primary air between 3.0 and 4.0, highlighting that higher secondary air velocities led to a better mixture between secondary air and producer gas. Therefore, the combustion efficiency increases because of the better mixture conditions and, thus, CO emissions decrease.<sup>33,52</sup>

The cookstove specific emissions of CO, working with pellets under cold start—stage 1, reached values of 3.20 and 3.37 g/MJ<sub>d</sub> for the combustion chambers 1 and 2, respectively (Figure 3). This means that the specific emissions of CO increased by 5% for combustion chamber 2. Under the hot start—stage 1, the cookstove working with pellets released 2.25 g/MJ<sub>d</sub> of CO with combustion chamber 1 and 2.30 g/MJ<sub>d</sub> with combustion chamber 2 (2% increase with combustion chamber 2). Concerning the chips, a more noticeable difference was observed of the specific emissions of CO of the cookstove as a function of the combustion chambers. The specific emissions of CO of the cookstove under cold start—stage 1 was 2.81 g/MJ<sub>d</sub> with combustion chamber 1 and 3.25 g/MJ<sub>d</sub> with combustion chamber 2 (specific emissions of CO was 14% higher with combustion chamber 2), see Figure 3. Whereas under hot start—stage 1, the specific emissions of CO was 2.13 g/MJ<sub>d</sub> with combustion chamber 1 and 2.81 g/MJ<sub>d</sub> with combustion chamber 2. That is equivalent to a 24% increase in the specific emissions of CO for combustion chamber 2. As it is analyzed in Section 2.2, the lower Reynolds number (*Re*) of the combustion air in combustion chamber 2 inhibits the mixture between the combustion air and the producer gas.<sup>47</sup> This, in turn, leads to decrease the oxygen and temperature in the combustion zone, and consequently, the CO emissions increase.<sup>52,61</sup>

Finally, concerning the start type, the cookstove with pellets reached specific emissions of CO values of 3.28 g/MJ<sub>d</sub> under

cold start—stage 1 and 2.27 g/MJ<sub>d</sub> under hot start—stage 1 (Figure 3), corresponding to a 45% reduction in the specific emissions of CO from cold start—stage 1 to hot start—stage 1. For the chips, the specific emissions of CO decreased by 23% from cold start—stage 1 to hot start—stage 1, whose values were 3.03 and 2.47 g/MJ<sub>d</sub>, respectively. This behavior is a consequence of the cookstove preheating in hot start—stage 1, which favored the gasification process leading to reach higher temperatures of the producer gas. Thereby, the oxidation reactions in the combustion zone are favored, while the CO emissions diminish.<sup>62</sup> Furthermore, another aspect that favors a higher temperature in the oxidation zone of the producer gas under hot start—stage 1 is the higher CO and CH<sub>4</sub> concentrations produced during the gasification process in this stage. The higher CO and CH<sub>4</sub> concentrations are related to a higher quantity of energy and a higher oxidation temperature (see Section 2.3).

It is highlighted that the reduction of the specific emissions of CO achieved with gasification-based cookstoves might contribute to achieve the pollutant emission levels established by the WHO for IAQ. The specific emissions of CO that achieve the WHO standards might be possible through a set of variations in the cookstove design, and more specifically, with the variation of the design of the combustion chamber.<sup>61</sup>

**Specific Emissions of Total Suspended Particle Matter— $EF_{TSPM}$  (mg/MJ<sub>d</sub>) with Pellets:** The emissions of total suspended particle matter of the TLUD cookstove using pellets as fuel are shown in Figure 5. According to the ANOVA (Figure 6), the

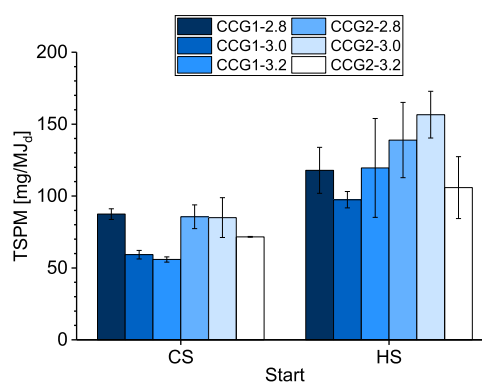


**Figure 5.** Specific emissions of total suspended particle matter— $EF_{TSPM}$  (mg/MJ<sub>d</sub>) of the gasification-based cookstove with pellets as a function of start type (cold start, hot start).

only factor that has a statistically significant effect on the specific emissions of total suspended particle matter is the start time (cold start and hot start). The combustion-air/gasification-air ratio and the combustion chamber design do not statistically affect the specific emissions of the total suspended particulate matter. In particular, the combustion chamber factor in the cold start reached an average specific emissions of total suspended particle matter of 67.5 mg/MJ<sub>d</sub> with combustion chamber 1 and 80.73 mg/MJ<sub>d</sub> with combustion chamber 2. This corresponds to ~20% reduction of the total suspended particulate matter emissions with combustion chamber 1. Similarly, under the hot start, the specific emissions of total suspended particle matter were ~20% lower with combustion chamber 1, with average values of 111.64 and 133.77 mg/MJ<sub>d</sub> for combustion chamber 1 and combustion chamber 2, respectively. According to Kshirsagar and Kalamkar,<sup>47</sup> the total suspended particulate matter specific

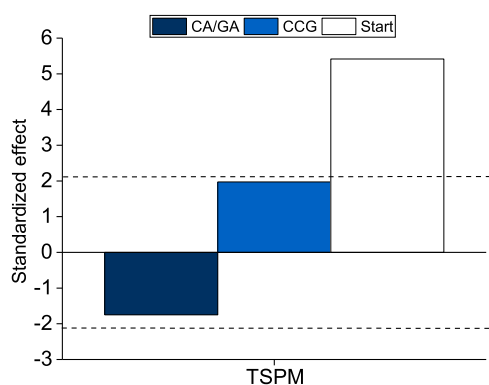


**Figure 6.** Pareto chart: effect of combustion-air/gasification-air ratio, combustion chamber CCG, and start type on specific emissions of total suspended particle matter— $EF_{TSPM}$  (mg/MJ<sub>d</sub>) from the TLUD cookstove using pellets as fuel.

emissions as a function of the combustion chamber decrease with a higher turbulence in the combustion air flow because the mixing between the producer gas and the combustion air is improved. As it is analyzed in Section 2.2, the weighted Reynolds number for combustion chamber 1 reached a value  $\sim 11\%$  higher than that of combustion chamber 2. Therefore, the specific emissions of total suspended particle matter decreases for combustion chamber 1 because this combustion chamber fosters a better mixing between the producer gas and combustion air.

The start factor had average values of 74.11 mg/MJ<sub>d</sub> in cold start and 122.70 mg/MJ<sub>d</sub> in hot start, which accounts for 40% fewer emissions of total suspended particulate matter in cold start. The higher amount of total suspended particulate matter released in the hot start is attributed to the higher biomass/air equivalence ratio reached in the hot start (Section 2.3), which promotes a higher concentration of tars in the producer gas, whose species are precursors of particulate matter formation.<sup>63</sup>

Comparing the total suspended particulate matter emissions of traditional cookstoves whose values ranged from 219 to 347 mg/MJ<sub>d</sub>,<sup>45,64</sup> the TLUD cookstove studied herein reached reductions between 65 and 80%. Furthermore, the values obtained in the total suspended particulate matter emissions are comparable to other improved cookstoves with wood as fuel, whose values ranged from 105 to 207 mg/MJ<sub>d</sub>.<sup>4,45,46,50,64</sup>

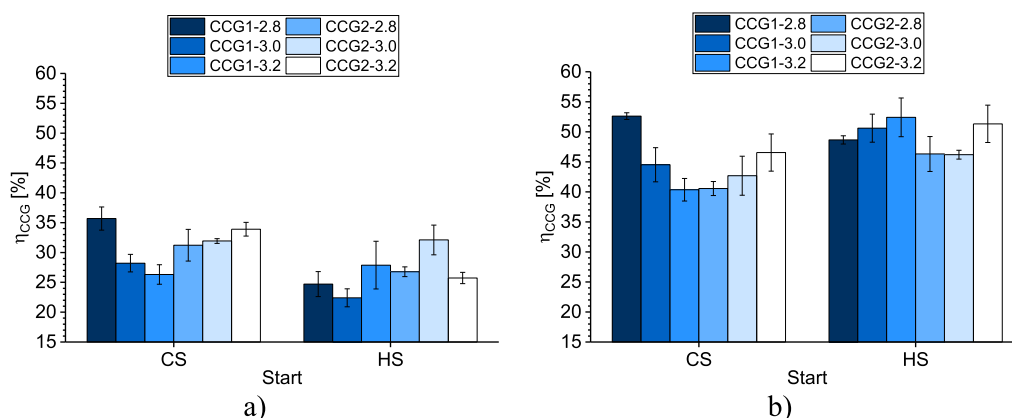


**Figure 7.** Energy efficiency of the combustion chamber ( $\eta_{CCG}$ , %) as a function of the controllable parameters of the cookstove. (a) Pellets and (b) chips.

**2.2. Control Volume 2: Combustion Chamber. Energy Efficiency.** The control volume 2 is characterized by the energy efficiency of the combustion chamber ( $\eta_{CCG}$ ) as a function of the controllable factors in the cookstove (Figure 7), such as biomass density (560 kg/m<sup>3</sup> for pellets and 151 kg/m<sup>3</sup> for chips), combustion-air/gasification-air ratio (2.8, 3.0, and 3.2), the design of the combustion chamber (combustion chambers 1 and 2), and the start mode of the WBT protocol (cold start and hot start). In Figure 8, the analysis of variance through the

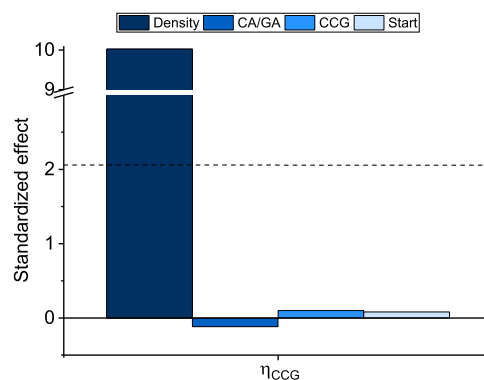


**Figure 8.** Pareto chart: energy efficiency of the combustion chamber— $\eta_{CCG}$  (control volume 2) of the gasification-based cookstove as a function of controllable parameters.

Pareto chart is presented, showing the significance of the analyzed factors on the energy efficiency of the combustion chamber with a confidence level of 95%.

According to the ANOVA, the biomass density has a statistically significant effect on the energy efficiency of the combustion chamber (Figure 8). For the fuel type, it is worth noting that the chips (151 kg/m<sup>3</sup>) reached an average value of energy efficiency of the combustion chamber  $\sim 53\%$  higher than that of the pellets (560 kg/m<sup>3</sup>), with average values of 43.84 and 28.61%, respectively (Figure 7a,b). The power supplied to the water ( $P_w$ , kW) does not show a significant difference when varying the biomass density because the volume was set at 3 L (eq 2). Therefore, the result of the energy efficiency of the combustion chamber is attributed to the power of the producer gas ( $P_{pg}$ , kW). The power of the producer gas of the chips was 4.97 kW, which is directly related to the lower volumetric flow ( $\dot{V}_{pg}$ , N m<sup>3</sup>/h) and the heating

value of the producer gas, while the power of the producer gas from the pellets was 6.78 kW (eq 3). Therefore, when the denominator decreases for the chips in eq 1, and the numerator is constant (power delivered to the water), consequently, the efficiency increases. The gasification process in the cookstove is explained in detail in Section 2.3.

The energy efficiency of the combustion chamber as a function of the combustion-air/gasification-air ratio does not present a specific trend (Figure 7). Besides, the combustion-air/gasification-air ratio does not have a statistically significant effect on the energy efficiency of the combustion chamber (Figure 8). This behavior is explained through the velocity fields (Supporting Information S4) and the Reynolds number— $Re$  (Figure 9) estimated through CFD simulation

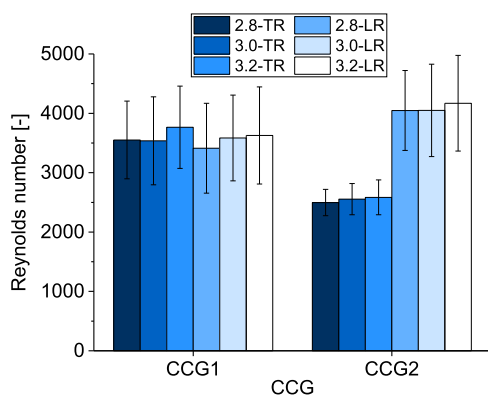


**Figure 9.** Average Reynolds number of the combustion air flow through the top and low rows of combustion chamber 1 (CCG1) and combustion chamber 2 (CCG2) as a function of the different combustion-air/gasification-air ratios (2.8, 3.0, and 3.2).

for both combustion chambers (see Figure 13) and for the combustion-air/gasification-air ratios (2.8, 3.0, and 3.2). The variation of the average  $Re$  as a function of the combustion-air/gasification-air ratio is below 6% in each row (top row—TR and lower row—LR) of the combustion chambers (Figure 9). According to this mild variation, it is stated that the combustion air flow conditions are similar; therefore, the variation of the energy efficiency of the combustion chamber as a function of the combustion-air/gasification-air ratio is not significant.

The weighted  $Re$  of each combustion chamber corresponds to the sum of the products between the  $Re$  of each row of grooves and their corresponding area percentage of combustion air output. This means,  $Re_{\text{weighted}} = \sum Re_i \times AP_i$ , with  $i = \text{TR and LR}$ ; for combustion chamber 1,  $AP_{\text{TR}} = AP_{\text{LR}} = 50\%$ , and for combustion chamber 2,  $AP_{\text{TR}} = 60\%$ , and  $AP_{\text{LR}} = 40\%$ . The weighted  $Re$  reached a value of 3579 for combustion chamber 1, while for combustion chamber 2, a value of 3214 was obtained. This means that the  $Re$  of combustion chamber 1 is  $\sim 11\%$  higher compared to that of combustion chamber 2, which promotes a better mixing between the producer gas and the combustion air in combustion chamber 1, producing lower CO emissions in the TLUD cookstove.<sup>33</sup> The magnitudes of the weighted  $Re$  indicated that the combustion air flow is found in the transition zone in both combustion chambers.<sup>65</sup> The variation of the  $Re$  standard deviation is a consequence of the velocity field of the combustion air at the exit of the grooves of the combustion chambers (Figure 9), which varies

up to 3 m/s in a same groove due to geometry, see Figures S1 and S2 (Supporting Information S4).

Concerning the start mode, it was found that this factor does not have a statistically significant effect on the energy efficiency of the combustion chamber (Figure 8). However, the energy efficiency of the combustion chamber decreased by  $\sim 17\%$  from cold start to hot start for the pellets, with average values of 31.21 and 26.6%, respectively. An opposite trend was found with the chips because the energy efficiency of the combustion chamber increased from 44.55 to 49.25% from cold start to hot start. The behavior for the pellets is related to an increase of the  $\sim 21\%$  in the power of the producer gas, when going from 5.99 kW in cold start to 7.56 kW in hot start. This is ascribed to an increase of  $\sim 4\%$  in the volumetric flow of the producer gas (7.78 N m<sup>3</sup>/h in cold start, and 8.14 N m<sup>3</sup>/h in hot start) and  $\sim 17\%$  in the heating value of the producer gas reached with the preheated cookstove (2.76 MJ/m<sup>3</sup> in cold start, and 3.33 MJ/m<sup>3</sup> in hot start), see Section 2.3. Furthermore, the increase in the power of the producer gas is  $\sim 76\%$  higher than the increase of thermal power of boiled water ( $P_w$ ) using pellets under the hot start. The thermal power of boiled water increases by  $\sim 4\%$  when going from 1.88 kW in cold start to 1.96 kW in hot start; thereby as the denominator of eq 1 increases, the energy efficiency of the combustion chamber decreases.

For the chips, the thermal power of boiled water increased by  $\sim 13\%$  when going from cold start to hot start, while the powers of the producer gas reached were 4.73 and 5.24 kW for cold start and hot start, respectively. As a consequence, the rise in thermal power of boiled water is  $\sim 36\%$  higher than the increase in the power of the producer gas with the preheated cookstove, favoring the energy efficiency of the combustion chamber (eq 1). The higher value reached for the thermal power of boiled water might be attributed to a decrease of  $\sim 14\%$  in the test time, which varies from 497 s in cold start down to 435 s in hot start. Although for the chips, the volumetric flow and the heating value of the producer gas increased by  $\sim 2$  and  $\sim 8\%$ , respectively, during the hot start, these rises are lower than the increment noted in the power of the water because of the shorter test time. This explains the improvement observed for energy efficiency of the combustion chamber with chips.

The efficiency values found in the combustion chambers with chips—control volume 2 (not for the cookstove in its global ensemble) are close to the efficiencies presented in the Clean Cooking Catalog of Clean Cooking Alliance for cookstoves that work with LPG as fuel ( $\sim 49\%$  efficiency).<sup>59</sup> Comparing to other cookstoves that work with other gaseous biofuels such as biogas, the thermal efficiency reached with chips (43.84% on average) is similar to the ones reported by Sukhwani et al.<sup>66</sup> and by Demissie et al.<sup>67</sup> with values of 43 and 43.6%, respectively. This result is mainly attributed to the lower power of the producer gas obtained using the chips, which is reflected in the increase of the energy efficiency of the combustion chamber. Meanwhile, other cookstoves using biogas under WBT protocol and with improved designs of burners have reached efficiencies of 56.89<sup>68</sup> and 67.01%.<sup>69</sup>

**2.3. Control Volume 3: Gasification Process.** The control volume 3 corresponds to the gasification process of the pellets and chips in the cookstove bed, which represents a TLUD-type or reverse downdraft-type reactor at atmospheric pressure. The gasifying agent is air at a fixed rate of 0.12 kg/m<sup>2</sup>/s for both biomasses. Figure 10 shows the characteristic

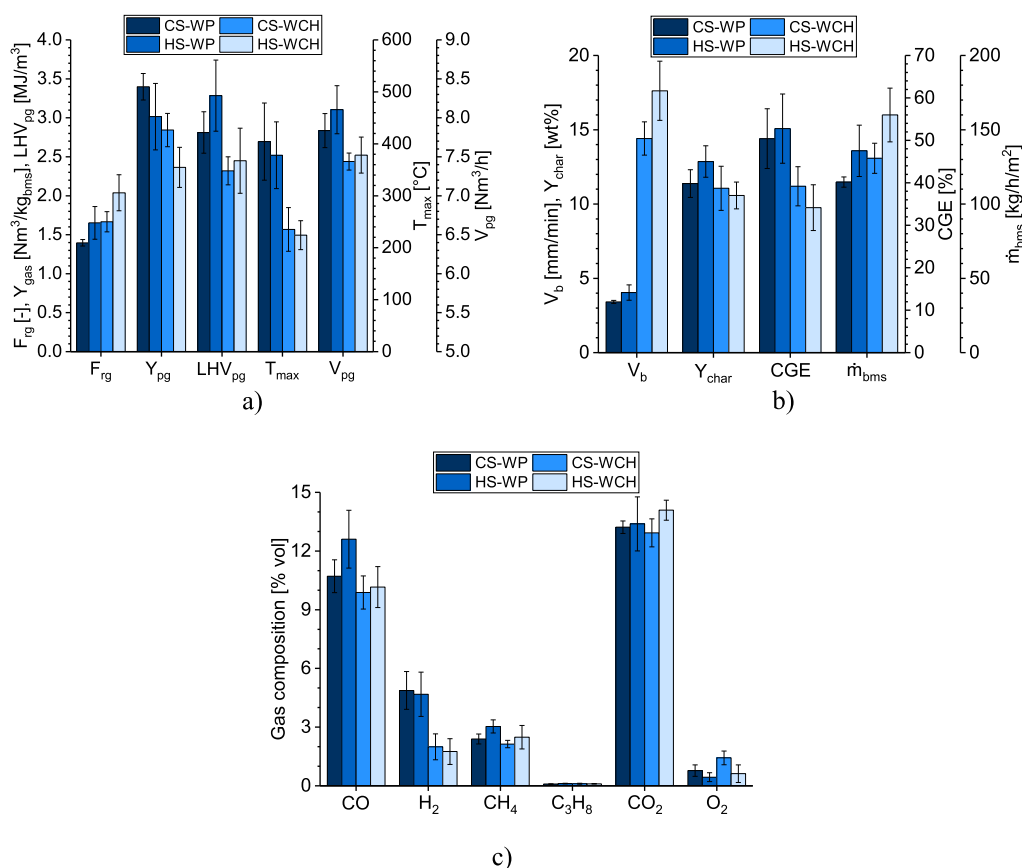


**Figure 10.** Parameters of the gasification process for the pellets and the chips as a function of the start type, cold start (CS) and hot start (HS). (a) fuel/air equivalence ratio— $F_{rg}$  (-), producer gas yield— $Y_{pg}$  ( $Nm_{pg}^3/kg_{bms}$ ), heating value of the producer gas— $LHV_{pg}$  ( $kJ/Nm^3$ ), process maximum temperature— $T_{max}$  ( $^{\circ}C$ ), and volumetric flow of the producer gas— $V_{pg}$  ( $Nm^3/h$ ); (b) biomass burning velocity— $V_b$  (mm/min), biochar mass yield— $Y_{char}$  (%), cold gas efficiency—CGE (%), and biomass consumption rate— $m_{bms}$  ( $kg/h/m^2$ ); and (c) producer gas composition on dry basis (% vol).

parameters of the gasification process, such as process maximum temperature ( $^{\circ}C$ ) measured close to the reactor wall (Section 4.5), fuel/air or biomass/air equivalence ratio (dimensionless), and biomass burning velocity (mm/min). Besides, biomass consumption rate ( $kg/h/m^2$ ), the dry base composition (% vol) and volumetric flow ( $Nm^3/h$ ) and heating value ( $kJ/Nm^3$ ) of the producer gas, cold gas efficiency (%), producer gas yield ( $Nm_{pg}^3/kg_{bms}$ ), and biochar mass yield (% wt). In Figure 11, the statistical results are shown through a Pareto chart for each of the response variables analyzed as a

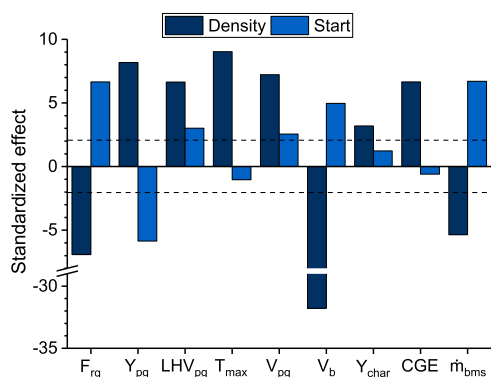


**Figure 11.** Pareto chart: effects of biomass density and start type on the gasification process parameters.

function of the considered factors, biomass density (pellets and chips) and the process start type (cold start and hot start). Representing the ANOVA with a confidence interval of 95%, the effect of the producer gas species is reflected in the heating value of the producer gas; therefore, the heating value of the producer gas is statistically analyzed instead of every gaseous species.

According to the ANOVA, the biomass density has a statistically significant effect on process maximum temperature (Figure 11). The process maximum temperature of the pellets ( $391.07^{\circ}C$ ) was  $\sim 70\%$  higher on average concerning the temperature reached with the chips ( $229.70^{\circ}C$ ), as observed in Figure 10a. The heat release rate of pellets into the bed increased because of its higher heating value ( $19.03 MJ/kg$ ) compared to that for the chips ( $16.85 MJ/kg$ ) (Table 1). Furthermore, the higher packing factor of the pellets (packing factor equal to 0.48, Table 1) than that of the chips (packing factor equal to 0.36, Table 1)<sup>70</sup> promotes a higher absorption of the radiative heat transference in the solid phase of the pellets.<sup>19,71</sup> The higher absorption of the radiation intensity favors a higher energy concentration in the reaction front, which leads to an increase in the temperature reached for the pellets. Although the start type does not have a statistically significant effect on process maximum temperature (Figure 11), there was a slight decrease of process maximum temperature in both biomass for the hot start compared to the cold start, which is related to the increase in the fuel/air

equivalence ratio in hot start due to the higher biomass consumption rate (Figure 10a,b), resulting in a lower temperature in the reaction front.<sup>19</sup>

The biomass density and the start type have a statistically significant effect on fuel/air equivalence ratio (Figure 11), which increased by ~22% on average for the chips concerning the pellets (Figure 10a). This is attributed to the higher burning ( $V_b$ ) and the biomass consumption rates ( $\dot{m}_{bms}$ ) of the chips (Figure 10b).<sup>19,71</sup> The preheating of the reactor in the hot start favors the drying of the raw biomass, which reduces the energy requirements from the reaction front to process the fresh biomass. As a consequence, the reaction velocity and the biomass consumption rate increase.<sup>71</sup> Therefore, for the hot start, the fuel/air equivalence ratio increased by ~18% for the pellets and by ~22% for the chips compared to the cold start.

In this study, an opposite effect was found between the fuel/air equivalence ratio and producer gas compositions for these two types of biomass (Figure 10a,c). Even though the average fuel/air equivalence ratio for the pellets was 1.52 and 1.85 for the chips, a higher concentration of gaseous fuel species was reached for the pellets, whose average composition was 16, 18, and 155% higher for CO, CH<sub>4</sub>, and H<sub>2</sub>, respectively, concerning the gas composition of chips. The higher energy content of the pellets producer gas is ascribed to the higher reaction temperature reached with this biomass, which is favored by its higher bulk density. However, in Figure 10c a slight decrease in H<sub>2</sub> is observed when comparing cold start with hot start in both biomass types. The lower temperatures in the hot start tend to slightly reduce activation for producing H<sub>2</sub>; such as the cracking and the reforming of hydrocarbons and tars, and the char reduction with steam.<sup>72</sup> For both biomasses, CO and CH<sub>4</sub> tend to increase in hot start compared to the cold start. This behavior is related to the higher fuel/air equivalence ratio attributed to the increase of biomass burning velocity under the hot start (Figure 10a,b).<sup>70</sup>

Concerning biomass burning velocity, both factors have a statistically significant effect, although the higher effect is generated by the biomass density (Figure 11). Despite the lower temperature reached by the chips, the average biomass burning velocity of this biomass was 4.3 times higher than that reached by the pellets (Figure 10b). This behavior was attributed to the higher penetration of radiative heat transference in the solid phase of the chips, whose mechanism favors the drying and devolatilization processes of the raw biomass, thus fostering a higher reaction velocity.<sup>19,56</sup> As for the start type, from cold start to hot start, the biomass burning velocity increased by 35% for the pellets and by 22% for the chips. This is ascribed to the preheated process of the cookstove walls when the gasification process is carried out under hot start. The biomass density and the start type have a statistically significant effect on the biomass consumption rate (Figure 11). The biomass consumption rate reached a value of 145.39 kg/h/m<sup>2</sup> for the chips compared to the 125.33 kg/h/m<sup>2</sup> for the pellets (Figure 10b). The trend in the biomass consumption rate is similar to the one observed for the biomass burning velocity because both variables are correlated (eq 5).<sup>56</sup>

As a consequence of the higher concentration of gaseous fuel species reached by the pellets, its producer gas heating value increased by ~28% concerning the one from the chips, with average values of 3047.90 kJ/Nm<sup>3</sup> for the pellets and 2384.58 kJ/Nm<sup>3</sup> for the chips (Figure 10a). The higher concentration of combustible gaseous species reached for the pellets is

ascribed to their higher reaction temperature, which favored the reduction reactions ( $C + CO_2 \rightarrow 2CO$ ,  $C + 2H_2 \rightarrow CH_4$ , and  $C + H_2O \rightarrow CO + H_2$ ), and therefore, the production of combustible gaseous species.<sup>73</sup> The volumetric flow of the producer gas reached by the pellets was 7% higher than that of the chips, with values of 7.97 and 7.48 Nm<sup>3</sup>/h, respectively. The higher producer gas volumetric flow of the pellets is related to their higher bulk density (559.97 kg/m<sup>3</sup>, Table 1), which contributes to increase the biomass amount per volume unit of the reactor; thereby, the increment of the gas production is favored by mass conservation.

The biomass density and the start type have a statistically significant effect on the heating value and volumetric flow of the producer gas, the biomass density is the factor with the highest effect in both response variables (Figure 11). As for the cold gas efficiency, the biomass density statistically affects this parameter. The cold gas efficiency was in average 51.6% for the pellets and 36.7% for the chips (Figure 10b). This difference of ~41% is attributed to the higher flow and heating value of the producer gas, as well as to the lower biomass consumption rate (~16%) reached with the pellets. Therefore, the power associated with the producer gas increases while the energy supplied by the biomass to gasification process decreases, which leads to an increase in the cold gas efficiency.<sup>74</sup> In hot start, the increase of ~17% in the heating value of the producer gas for the pellets favored a rise of ~5% for cold gas efficiency compared to the cold start. While for the chips in hot start, the increase of ~6% in the heating value of the producer gas was not enough to compensate the increase of the biomass consumption rate (~22%) during this start, whereby the cold gas efficiency decreased by ~13% from cold to hot start.<sup>20</sup>

The biomass density and the start type statistically affect the producer gas yield (Figure 11). The producer gas yield was on average 23% higher for the pellets concerning that of chips. This is because the pellets reach a higher volumetric flow of the producer gas (~7%) and a lower biomass consumption rate (~16%). Concerning the effect of the start type, from cold to hot start, the producer gas yield decreased by 11% for the pellets and by 17% for the chips. This reduction is attributed to the fact that the increase of volumetric flow of the producer gas (3% for the pellets and 1% for the chips, from cold to hot start) is less significant than the increase reached by the biomass consumption rate, 18 and 22% for the pellets and the chips, respectively (Figure 10a).

The biomass density significantly affects the biochar mass yield (Figure 11). The pellets reached an average biochar mass yield of 12.12%, while that one obtained from the chips was 10.82% on average. The higher biochar yield for the pellets is due to their higher bulk density.<sup>53</sup> Furthermore, biomasses with a higher content of lignin tend to reach a higher biochar yield;<sup>75</sup> in this work, the lignin content for the pellets is ~12% higher than that for the chips (43.74 and 39.10 wt %, respectively).<sup>76</sup> With respect to the start type, from cold to hot start, biochar mass yield of the pellets increased by 13%, while biochar mass yield for the chips decreased by 4% (Figure 10b). This behavior is ascribed to the fibrous nature of the chips and its surface area (BET), which is ~4 times higher than that of the pellets,<sup>76</sup> which leads to favor the reactions of the gasification process, and consequently, the biochar mass yield decreases.

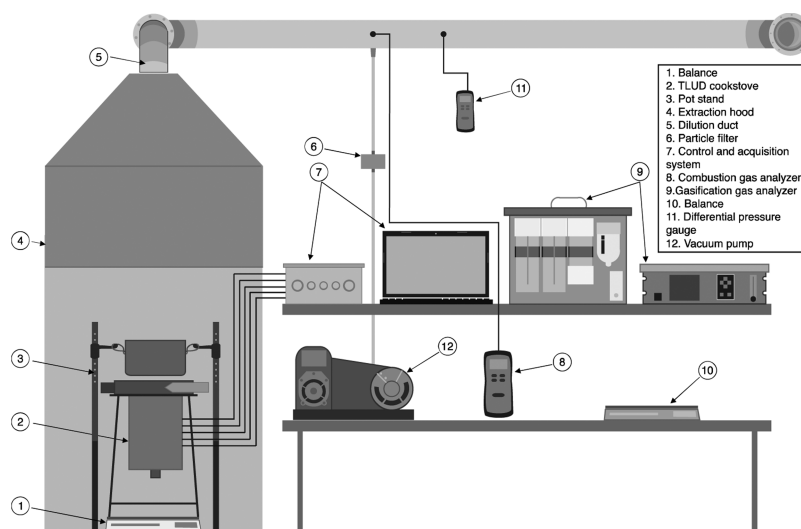


**Figure 12.** Experimental installation of the biomass gasification-based cookstove (TLUD).

### 3. CONCLUSIONS

The best performance of the gasification-based biomass cookstove, assessed here, was reached by using pellets as fuel, with values of 25.21%, 82.32 g/L, and 172.71 kJ/L·min for the efficiency, the specific energy consumption, and the specific energy consumption per unit time, respectively. This behavior accounts for efficiency, specific energy consumption, and specific energy consumption per unit time values of 5% higher, 7% lower, and 21% lower in comparison to the values reached with the TLUD cookstove using chips. According to the thermodynamic analysis carried out on the gasification process, the higher values in the bulk density, packing factor, and the heating value of the pellets, allowed for this fuel to reach higher temperatures in the gasification bed and a lower biomass consumption rate, which improved the composition and increased the heating value of the producer gas, as well as the cold gas efficiency, and the amount of energy transferred to the water. As a consequence, fostering the use of densified biomass as a fuel in gasification-based cookstoves is suitable. The efficiency values reached by the TLUD cookstove with pellets and chips, in comparison to the efficiencies reported for TSF cookstoves (10–14%) were 80 and 72% higher, respectively.

Concerning the pollutant emissions released, the carbon monoxide specific emissions were similar for the pellet and chip biomasses (2.78 g/MJ<sub>d</sub> for the pellets, and 2.75 g/MJ<sub>d</sub> for the chips) due to the fact that the biomasses used were derived from the same forest species (*Pinus patula*). On the other hand, an important effect of the combustion chamber design of the cookstove on the pollutant emissions was noted. For combustion chamber 1, a lower amount of CO and total suspended particulate matter (74.11–122.70 mg/MJ<sub>d</sub>) emissions were reached due to a higher turbulence in the combustion zone. The higher turbulence of the combustion air favors its mixing with the producer gas. Therefore, the combustion air in gasification-based stoves should be supplied to the combustion chamber in a turbulent regime in order to favor the mixing and the gas–gas combustion reaction. Thereby, the cookstove efficiency increases, while the pollutant emissions drop.

The combustion-air/gasification-air ratio (2.8, 3.0, and 3.2) did not have a significant effect on the energy performance and

pollutant emissions of the gasification-based biomass cookstove, whereby the cookstove is noted to be operate near the stoichiometric zone for the producer gas, which is the optimal point. The oxygen-lean reactions generate an incomplete combustion of the producer gas, while oxygen-rich reactions might cool the flame front. For both cases, oxygen-lean and -rich, the stove efficiency would be reduced while the CO and total suspended particulate matter emissions would increase. Regarding the TSF cookstoves, the TLUD gasification stove showed 82% lower CO emissions, and a reduction in the total suspended particulate matter emissions between 65 and 80%.

### 4. MATERIALS AND METHODS

In this work, the effect of three controllable parameters on the energy and environmental performance of a biomass gasification-based cookstove (or TLUD) is studied. The considered parameters are (i) the bulk density, using wood pellets and wood chips from pine patula as fuels; (ii) the combustion-air/gasification-air ratio considering the values of 2.8, 3.0, and 3.2; and (iii) the cookstove design through the variation of geometry in the combustion chamber of the producer gas. Two combustion chambers are evaluated (combustion chambers 1 and 2). The effect of the controllable parameters on three control volumes is analyzed. The control volumes are (1) the energy and the environmental performance of the TLUD cookstove; (2) the thermal efficiency of the combustion chamber of the producer gas; and (3) the thermodynamic performance of the gasification process in the cookstove. The experiments were conducted by combining the levels of the three factors, the experimental plan was replicated twice, for 24 tests following the modified WBT 4.2.3 protocol. The results obtained were analyzed through the analysis of variance to determine the factors that are statistically significant for the response variables.

**4.1. Biomass Samples Used as Fuel.** The biomass used was pine patula wood (*P. patula*) due to its dendroenergetic potential in Colombia. This is given by silvicultural properties, such as annual yield of ~20 m<sup>3</sup>/ha year, harvest time of ~13 years, and a planted area in the country of ~38,500 ha.<sup>77</sup> Wood chips and wood pellets were used, which are the most common products for energy generation and use in gasification-based cookstoves globally.<sup>78–80</sup> The chips were obtained in the

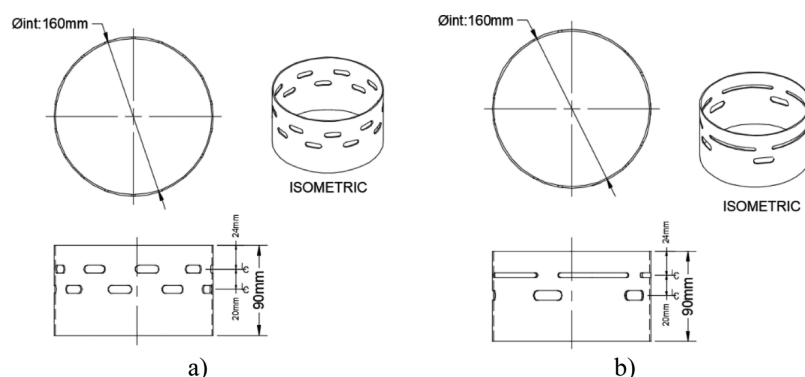


**Figure 13.** Combustion chambers for the producer gas oxidation in the TLUD cookstove. (a) design of combustion chamber 1, and (b) design of combustion chamber 2.

*Bandit 95XP* equipment with particle sizes between 4 and 20 mm, while the pellets were obtained commercially in a sawmill located in Medellín (Colombia). The pellets had a diameter of 8 mm and a length between 10 and 15 mm. This particle size is suitable for a stable oxidation in gasification processes.<sup>70,81</sup> Physicochemical properties of the two biomass types are presented in Table 1.

**4.2. Experimental Setup.** The experimental installation is composed of a gasification-based forced-draft cookstove, equipped both for executing performance tests under the WBT protocol and thermodynamic characterization of the gasification process. The different equipment that composes the experimental installation is shown in Figure 12.

Raw biomass is deposited and lit through the top of the reactor and, thus, the reaction front (or flame front) descends to the bottom part or grate. The gasification air is fed to the reactor through the bottom section and, therefore, the producer gas flow is opposed to the advance of the reaction front. During the gasification process, because of the stages of drying, pyrolysis, oxidation, and reduction of the biomass, the resulting products are producer gas and biochar.<sup>32</sup> The producer gas leaves the reactor through the top where the combustion chamber is located. At this point, the oxidation of the gas with the combustion air occurs. The energy released by the producer gas oxidation is used in the heating of water (simulating cooking) and polluting gases such as CO generated by incomplete combustion and particulate matter are released.

Constructively, the geometry of the reactor is cylindrical with an internal diameter of 0.16 m and a height of 0.28 m. Throughout the length of the reactor, there are five type-K thermocouples ( $\pm 1$  °C), separated every 0.04 m and inserted 5 mm into the bed. This insertion distance of the thermocouples was set to avoid the formation of preferential paths and have the ability to conduct WBT tests under cold start as well as hot start. The thermocouples are used to measure the temperature throughout the gasification bed. The gasification air is supplied through a duct of 0.04 m diameter and is driven by a GOSTIME 12 V—0.06A axial fan, with a fixed flow of  $146 \pm 4.35$  L/min ( $0.12$  kg/m<sup>2</sup>/s) for all the conducted experiments. At the top of the reactor, the combustion chamber is located (Figure 13). Combustion chamber 1 (Figure 13a) has an internal diameter of 0.16 m and two rows of grooves, each with nine grooves of height 8 mm and length 24 mm. Combustion chamber 2 shown in Figure 13b has an internal diameter of 0.16 m and two rows of grooves. The lower row has five grooves of 10 mm in height and 30 mm in length. The upper row is composed of five grooves of 5 mm in height and 79 mm

in length. Both combustion chambers had a total area for the combustion air outlet of 3209 mm<sup>2</sup>. Combustion air is supplied by two GOSTIME 5 V—0.14A axial fans, through two 0.04 mm diameter ducts, tangentially joined to the combustion chamber. The aim of these grooved combustion chambers is to generate turbulence in the combustion air in order to favor the mixing between the air and the producer gas, seeking to improve the homogeneous combustion. The fields of velocities for the combustion air in combustion chambers 1 and 2 are determined through a numerical simulation using Ansys 19.0 software. The level of turbulence is estimated with the velocity fields in each combustion chamber through the calculation of the Reynolds number.

The supervisory control and data acquisition system are composed of a National Instruments data acquisition card USB-6001 and a program developed with LabView. The five temperatures throughout the gasification bed are visualized and registered with these two components and the water temperature is monitored and registered through a LM35 sensor ( $\pm 0.5$  °C). Additionally, the voltage of the fans supplying both gasification air and combustion air are controlled to regulate the flow supplied. Finally, the evolution of the biomass mass during the WBT is measured through a MAG master P balance with a capacity of 30 kg ( $\pm 0.1$  g). Water masses are measured with a MAG HAW-10BH balance with a capacity of 10 kg ( $\pm 0.1$  g). During the execution of the test, the pot with water is separated from the cookstove with an additional base, as shown in Figure 12 (3. Pot stand), to measure biomass consumption and evaporated water mass independently.<sup>33</sup> The experimental installation is also composed by an extraction hood with a 0.8 m width, 1.0 m in length, and 2.0 m height, as shown in Figure 12 (4. Extraction hood). This is used for the extraction and measurement of combustion gases. The extraction hood is joined to a dilution duct with a diameter of 0.1 m. Extraction velocities in the hood are below 0.25 m/s, seeking to avoid air currents that interfere with the normal functioning of the cookstove.<sup>82</sup>

The composition of the producer gas (*syngas*) was measured using a Gasboard-3100 Serial (Cubic-Ruiyi Instrument) gas analyzer, which measures CO ( $\pm 2\%$  vol of full scale, non-dispersive infrared—NDIR), CO<sub>2</sub> ( $\pm 2\%$  vol of FS, NDIR), CH<sub>4</sub> ( $\pm 2\%$  vol of FS, NDIR), H<sub>2</sub> ( $\pm 3\%$  vol of FS, thermal conductivity detector—TCD), O<sub>2</sub> ( $\pm 3\%$  vol of FS, electrochemical detection—ECD), C<sub>3</sub>H<sub>8</sub> ( $\pm 2\%$  vol of FS, NDIR), and N<sub>2</sub> (calculated by difference). The composition of combustion gases was measured with a KIGAZ 310 (KIMO

Instruments) gas analyzer, with which it determined CO concentration ( $\pm 10$  ppm, by ECD), CO<sub>2</sub> (calculated), and gas temperature ( $\pm 1.1$  °C, type K thermocouple). The collection of total suspended particulate matter was carried out with Advantec GC-50 glass fiber filters with a diameter of 47 mm. The filters were conditioned with a temperature of  $20 \pm 3$  °C at a relative humidity of  $40 \pm 5\%$  during 24 h. The filters were installed in a filter holder fitted in a stainless-steel probe with 6.35 mm (1/4 in) of diameter and joined to a vacuum pump with a flow of  $24 \pm 0.5$  L/min. To calculate the gas flow in the dilution duct, a Pitot tube and Fieldpiece SDMN5 differential pressure manometer were used for measuring the dynamic ( $\pm 0.5$  mmWC) and the static pressures ( $\pm 0.5$  mmWC).

In this work, the TLUD cookstove is characterized as a function of three control volumes, as indicated in Figure 14.

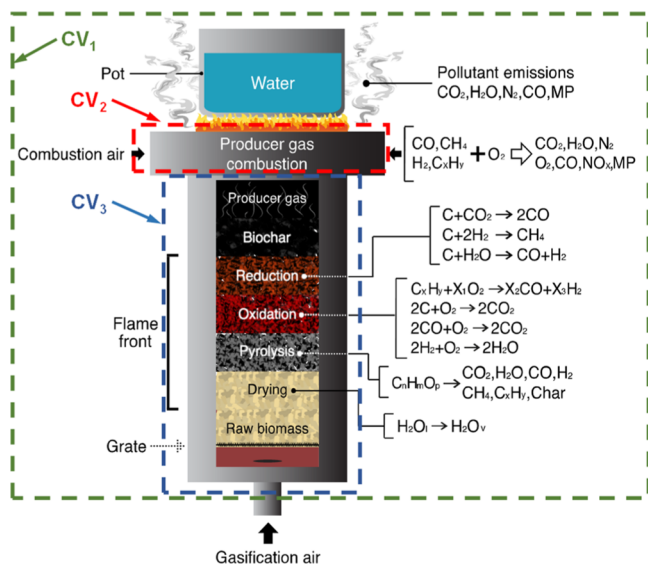


**Figure 14.** Stages, subprocesses, and control volumes that are part of the TLUD cookstove assessment.

Control volume 1 corresponds to the TLUD cookstove assessment following the WBT protocol. Control volume 2 contains the combustion chamber; and finally, control volume 3 considers the biomass gasification process of the cookstove.

#### 4.3. Control Volume 1: Gasification-Based Cookstove.

In this control volume, the TLUD cookstove is characterized under WBT protocol to determine (i) its energy performance: efficiency (%), specific energy consumption per unit time (kJ/L min), and (ii) pollutant emissions, such as specific emissions of CO (g/MJ<sub>d</sub>), and total suspended particulate matter (mg/MJ<sub>d</sub>).<sup>51,83</sup> The protocol for executing the experimental phase and the mathematical formulation for calculating the response variables associated with the cookstove performance are described below.

**4.3.1. Modified WBT Protocol.** TLUD cookstove is characterized following a modified WBT 4.2.3 protocol, which is shown in Figure 15. The original version of the WBT 4.2.3 protocol is proposed by the Clean Cooking Alliance.<sup>84</sup> It is worth noting that this modified WBT 4.2.3 protocol could be extended to assess other biomass cookstoves, seeking to carry out experimental tests under repeatability criteria, and with a useful method to enhance the data acquisition, such as particulate matter.

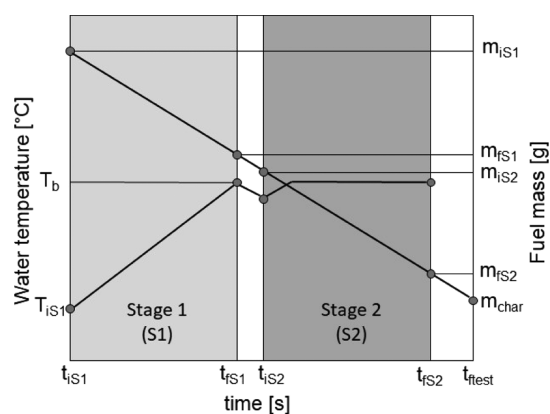


**Figure 15.** Modified 4.2.3 WBT protocol.

The WBT 4.2.3 protocol comprises two types of ignition to start the WBT tests.<sup>84</sup> These cookstove ignitions are cold start and hot start, both consisting in bringing water from room temperature to its boiling point. Here, each ignition, in turn, comprised two stages (stage 1 and stage 2), see Figure 15. Stage 1 of the cold start is indicated as cold start—stage 1. In this stage, the TLUD cookstove is turned on from room temperature (stove and water), and water (3 L) is brought to the boiling point ( $\sim 94$  °C for Medellín-Colombia). In stage 2 of the cold start (CS.S2), the boiling water is weighed and is put on the cookstove again. The objective of cold start—stage 2 is to extend the cookstove operation by simulating a long cooking time, while the energy yield but, most importantly, polluting emissions are registered and a higher amount of total suspended particulate matter is collected in the filter (Figure 12).

The hot start is conducted after finishing the cold start test. The cookstove is cleaned (biochar is weighted and removed), it is loaded again with raw biomass ( $\sim 1300$  g of pellets or 550 g of chips). The preheated cookstove is turned on and the pot with water (3 L) at room temperature is put on. The time elapsed between the cold start stage and the start of the hot start is below 10 min.<sup>84</sup> Stages 1 and 2 of the hot start are shown as hot start—stage 1 and hot start—stage 2, respectively. These stages are similar to the ones described for the cold start. The hot start—stage 1 starts with the preheated cookstove to boil water from room temperature. In hot start—stage 2, water continues to be boiled under the same conditions of biomass consumption, simulating a long and controlled cooking stage, obtaining more data related to performance, combustion gas concentration, and total suspended particulate matter. The procedure for executing cold start is presented in Table S1 (Supporting Information). At the end of the cold start stage, the biochar was removed and renewed the raw biomass load, following the same procedure indicated in Table S1 to carry out the hot start stage.

According to the modified WBT 4.2.3 protocol (Figure 15) during the execution of the tests, the following related variables are measured in each stages (Section S2, Supporting Information): initial water mass ( $m_{w,i}$  g), final water mass ( $m_{w,f}$  g), initial water temperature ( $T_{w,i}$  °C), final water temperature ( $T_{w,f}$  °C), initial fuel mass ( $m_{bms,i}$  g), final fuel mass ( $m_{bms,f}$  g), final biochar mass ( $m_{biochar}$  g), duration time of stage 1 ( $t_{s1}$ , s), duration time of stage 2 ( $t_{s2}$ , s), and duration time of the test ( $t_{test}$ , s). The WBT characterization of the TLUD cookstove as a function of controllable parameters was

carried out in two sections. In the first section, the three factors (biomass density, combustion-air/gasification-air ratio, and combustion chamber design) were studied through the execution of the modified WBT 4.2.3 protocol until the completion of stage 1 for both, the cold start and the hot start; that is, until water reaches the boiling temperature.<sup>47,51,57</sup> During this phase, the energy yield and the specific emissions of CO<sup>85</sup> were analyzed under these conditions. The second section was carried out while measuring the specific emissions of total suspended particle matter with pellets because this biomass type reached a better energy performance and lower pollutant emissions according to the first study described above.

**4.4. Control Volume 2: Combustion Chamber.** The control volume 2 was defined in order to analyze the  $\eta_{CCG}$  (%), calculated as expressed in eq 1. Here, the effects of the biomass bulk density (560 kg/m<sup>3</sup> for pellets, and 151 kg/m<sup>3</sup> for chips), the combustion-air/gasification-air ratio (2.8, 3.0, and 3.2), the design of the combustion chamber (combustion chambers 1 and 2), and WBT protocol start (cold start and hot start) are assessed.

$$\eta_{CCG} = \frac{P_w}{P_{pg}} \quad (1)$$

where  $P_w$  (kW) is the thermal power associated to boil the water (eq 2), and  $P_{pg}$  (kW) is the power of the producer gas (eq 3). The volumetric flow ( $\dot{V}_{pg}$ ) and the lower heating value of the producer gas (LHV<sub>pg</sub>) are calculated in Section 4.5.

$$P_w = \frac{E_{w,t_{s1}} + E_{w,t_{s2}}}{t_{s1} + t_{s2}} \quad (2)$$

$$P_{pg} = \dot{V}_{pg} \bullet LHV_{pg} \quad (3)$$

**4.5. Control Volume 3: Gasification Process.** The thermodynamic performance of the biomass gasification process in the TLUD cookstove (control volume 3) is characterized as a function of the biomass density (560 kg/m<sup>3</sup> for the pellets and 151 kg/m<sup>3</sup> for the chips) and the type of cookstove start (cold start and hot start). The experimental factors, such as the combustion-air/gasification-air ratio and the combustion chamber, are not considered in this analysis because control volume 3 corresponds to the gasification process (control volume 3 has its limit just before the combustion chamber, as shown in Figure 14). In this work, the parameters that characterize the TLUD gasification process are process maximum temperature (°C) measured near the reactor wall, fuel/air or biomass/air equivalence ratio (dimensionless), biomass burning velocity (mm/min), biomass consumption rate (kg/h/m<sup>2</sup>), composition on dry base (% vol) and volumetric flow of the producer gas (Nm<sup>3</sup>/h) and heating value of the producer gas (kJ/Nm<sup>3</sup>), cold gas efficiency (%), producer gas yield (Nm<sup>3</sup>/kg<sub>bms</sub>), and biochar mass yield (% wt). The values of fuel/air equivalence ratio (-), heating value of the producer gas (kJ/Nm<sup>3</sup>), and cold gas efficiency (%) were carried out following the methodology proposed by Diez et al.<sup>74</sup> The process maximum temperature (°C) was measured using the thermocouples located throughout the reactor, which shows a temperature close to the reactor walls. The biomass consumption rate by a unit of area  $\dot{m}_{bms}$  (kg/h/m<sup>2</sup>) was calculated through eq 4.

$$\dot{m}_{bms} = \frac{m_{bms}}{A_T} \quad (4)$$

where  $m_{bms}$  (kg/h) is the biomass consumption, which corresponds to the slope in the curve between the mass registered by the MAG master P scale and the time elapsed during the test execution.  $A_T$  (m<sup>2</sup>) is the reactor cross section (0.0201 m<sup>2</sup>).  $V_b$  (mm/min) is the ratio between  $\dot{m}_{bms}$  and the biomass bulk density ( $\rho$ , kg/m<sup>3</sup>) (eq 5).

$$V_b = \frac{\dot{m}_{bms}}{\rho_{bms}} \quad (5)$$

$Y_{pg}$  (Nm<sup>3</sup>/kg<sub>bms</sub>) was calculated by eq 6, which relates the volumetric flow of the producer gas ( $\dot{V}_{pg}$  Nm<sup>3</sup>/h) and biomass consumption rate  $m_{bms}$  (kg/h).<sup>88</sup>

$$Y_{pg} = \frac{\dot{V}_{pg}}{m_{bms}} \quad (6)$$

where  $\dot{V}_{pg}$  (Nm<sup>3</sup>/h) was obtained from N<sub>2</sub> mass balance between the producer gas and the N<sub>2</sub> in the air.<sup>71</sup> Finally, biochar mass yield (%) corresponds to the biochar yield calculated using the modified WBT 4.2.3 protocol, with eq S8.

**4.6. Experimental Conditions.** The experimental campaign of the TLUD cookstove is carried out randomly, keeping the place (Medellín-Colombia), the gasification cookstove, the measurement equipment, and the technical staff fixed in order to reduce the experimental error.<sup>87</sup> Additionally, the repeatability of the experimental installation was addressed by means of the variation coefficient and ANOVA, highlighting that the TLUD cookstove is a repeatable experimental unit with a variation coefficient <5.0%, and with 95% of confidence level.<sup>88</sup>

The starting main parameters considered in each test under the modified WBT 4.2.3 protocol are the initial water mass ( $m_{w,i}$  g), the initial water temperature ( $T_{w,i}$  °C), and the initial biomass mass ( $m_{bms,i}$  g). The tests were executed considering an initial water volume equivalent to 3 L.<sup>84</sup> An initial biomass mass is used for stage 1, both for the cold start and the hot start of ~1300 g for pellets, and ~550 g for chips. This difference is due to the bulk density of each fuel type (Table 1).

The fans for supplying the gasification air and combustion air were characterized before the experimental campaign in order to set voltages equivalent to the combustion-air/gasification-air ratios (2.8, 3.0 and 3.2) by controlling the flow through the data acquisition and control system (Figure 12). The gasification air flow was kept fixed for the experiments, 146 ± 4.35 L/min, equivalent to an air superficial velocity of 0.12 m/s, which corresponds to gasification regimes.<sup>81</sup> The air volumetric flow supplied by the fans for the combustion of the producer gas was 408.8, 438.0, and 467.2 L/min for ratios equal to 2.8, 3.0, and 3.2, respectively. The biomass used as fuel was *P. patula* wood in pellets and chips (Section 4.1). Finally, the producer gas combustion was carried out through the combustion chambers described in Section 4.2.

## ■ ASSOCIATED CONTENT

### Supporting Information

The Supporting Information is available free of charge at <https://pubs.acs.org/doi/10.1021/acsomega.1c05137>.

Procedure for executing the modified WBT 4.2.3 protocol, calculation model of WBT parameters, statistical experimental design, velocity fields of the combustion-air through the combustion chambers (CFD simulations), and the specific energy consumption of the TLUD cookstove (PDF)

## AUTHOR INFORMATION

### Corresponding Author

Juan F. Pérez – Grupo de Manejo Eficiente de la Energía—GIMEL, Facultad de Ingeniería, Universidad de Antioquia, Medellín 050010, Colombia; [orcid.org/0000-0002-3811-4471](https://orcid.org/0000-0002-3811-4471); Email: [juanpb@udea.edu.co](mailto:juanpb@udea.edu.co)

### Authors

Jonatan Gutiérrez – Grupo de Manejo Eficiente de la Energía—GIMEL, Facultad de Ingeniería and Grupo Energía Alternativa—GEA, Facultad de Ingeniería, Universidad de Antioquia, Medellín 050010, Colombia; [orcid.org/0000-0001-7532-8519](https://orcid.org/0000-0001-7532-8519)

Edwin Lenin Chica – Grupo Energía Alternativa—GEA, Facultad de Ingeniería, Universidad de Antioquia, Medellín 050010, Colombia; [orcid.org/0000-0002-5043-6414](https://orcid.org/0000-0002-5043-6414)

Complete contact information is available at: <https://pubs.acs.org/10.1021/acsomega.1c05137>

### Notes

The authors declare no competing financial interest.

## ACKNOWLEDGMENTS

The authors acknowledge the financial support of the Universidad de Antioquia through the research project PRG2020-33302.

## NOMENCLATURE

ANOVA	Analysis of Variance
AP	percentage of combustion-air outlet area, %
$A_T$	reactor cross section, $m^2$
CA	combustion air, L/min
CA/GA	combustion-air/gasification-air ratio
CCG	combustion chamber
CFD	fluid dynamic simulation
CGE	cold gas efficiency, %
CO	carbon monoxide
COPD	chronic obstructive pulmonary disease
$C_{p,water}$	specific heat of water, kJ/kg-K
CS	cold start
CS.S1	cold start—stage 1
CS.S2	cold start—stage 2
CV	control volume
$EF_{CO}$	specific emissions of CO, g/MJ <sub>d</sub>
$EF_{TSPM}$	specific emissions of total suspended particle matter, mg/MJ <sub>d</sub>
$E_{e,w,bms}$	energy to evaporate the moisture from biomass, J
$E_{s,bms}$	energy supplied by the biomass to boil-evaporate water, J
$E_{w,b}$	energy of boiled water, J
$E_{w,e}$	energy evaporated water, J
$E_{w,t}$	total energy supplied to the water, J
$F_{rg}$	fuel/air or biomass/air equivalence ratio, dimensionless
FS	scale factor

GA	gasification air, L/min
GDP	gross domestic product
$h_g$	latent heat of water evaporation, kJ/kg
HHV	higher heating value, kJ/kg
HS	hot start
HS.S1	hot start—stage 1
HS.S2	hot start—stage 2
IAQ	indoor air quality
LHV	lower heating value, kJ/kg
LPG	liquid petroleum gas
LR	lower row
$m_{biochar}$	biochar mass, g
$\dot{m}_{bms}$	biomass consumption rate, kg/h·m <sup>2</sup>
$m_{bms,c}$	mass of biomass consumed, g
$m_{bms,c,d}$	dry mass of biomass consumed, g
$m_{bms,f}$	final biomass mass, g
$m_{bms,i}$	initial biomass mass, g
$m_c$	biochar mass, g
MC	moisture content of biomass, % wt
$m_{ce}$	mass of the pot, g
$m_{CO}$	mass of CO, g
$m_{TSPM}$	mass of total suspended particle matter, mg
$m_{w,b}$	mass of boiling water, g
$m_{w,e}$	mass of evaporated water, g
$m_{w,f}$	final water mass, g
$m_{w,i}$	initial water mass, g
NDIR	non-dispersive infrared
PM	particulate matter
$P_{pg}$	power of the producer gas, kW
$P_w$	thermal power associated to boil the water, kW
Re	Reynolds number
S1	stage 1
S2	stage 2
SFCT	specific energy consumption per unit time, kJ/L·min
SFEC	specific energy consumption, kJ/L
TCD	thermal conductivity detector
$T_{d,bms}$	biomass drying temperature, °C
$T_{max}$	process maximum temperature, °C
TR	top row
$t_{s1}$	time spent during the stage 1, s
$t_{s2}$	time spent during the stage 2, s
$t_{test}$	duration time of the test, s
$T_{w,f}$	final water temperature, °C
$T_{w,i}$	initial water temperature, °C
TLUD	top-lit updraft cookstoves
TSF	traditional three stone fire
TSPM	total suspended particle matter
$V_b$	biomass burning velocity, mm/min
$\dot{V}_{duct}$	volumetric flow of gases flowing through the dilution line, m <sup>3</sup> /s
$\dot{V}_{pg}$	volumetric flow of the producer gas, Nm <sup>3</sup> /h
$\dot{V}_{vacuum\ pump}$	volumetric flow of gases flowing through the vacuum pump, m <sup>3</sup> /s
WBT	water boiling test
WCH	wood chips
WHO	World Health Organization
WP	wood pellets
$Y_{biochar}$	biochar mass yield, %
$y_i$	response variable
$Y_{pg}$	producer gas yield, Nm <sub>pg</sub> <sup>3</sup> /kg <sub>bms</sub>

## ■ GREEK SYMBOLS

$\varepsilon_{ij}$	error
$\eta$	thermal efficiency, %
$\eta_{CCG}$	combustion chamber energy efficiency, %
$\mu$	global measure
$\rho_{bms}$	biomass bulk density, kg/m <sup>3</sup>
$\rho_w$	water density, kg/m <sup>3</sup>
$\tau_i$	effect of factor $i$

## ■ REFERENCES

- (1) Lombardi, F.; Riva, F.; Bonamini, G.; Barbieri, J.; Colombo, E. Biomass and Bioenergy Laboratory Protocols for Testing of Improved Cooking Stoves (ICSts): A Review of State-of-the-Art and Further Developments. *Biomass Bioenergy* **2017**, *98*, 321–335.
- (2) Ramírez Quirama, J. F.; Tabora Vergara, A. L. Consumo de Leña En Fogones Tradicionales En Familias Campesinas Del Oriente Antioqueño. *Prod. + Limpia* **2014**, *9*, 99–114.
- (3) Manoj Kumar, M.; Sachin Kumar, S.; Tyagi, S. K. Design, Development and Technological Advancement in the Biomass Cookstoves: A Review. *Renewable Sustainable Energy Rev.* **2013**, *26*, 265–285.
- (4) Paulsen, A. D.; Garland, C.; Lascrain, J.; Kunsu, T. A.; Rossanese, M.; Jagoe, K.; Carpenter, A. L.; Méndez-Vides, A.; Delapena, S.; Yelvington, P. E. Emission Performance and User Acceptance of a Catalytic Biomass Cookstove in Rural Guatemala. *ACS Omega* **2019**, *4*, 2981–2988.
- (5) Stanaway, J. D.; Afshin, A.; Gakidou, E. Global, Regional, and National Comparative Risk Assessment of 84 Behavioural, Environmental and Occupational, and Metabolic Risks or Clusters of Risks for 195 Countries and Territories, 1990–2017: A Systematic Analysis for the Global Burden of Disease Study 2017. *Lancet* **2018**, *392*, 1923–1994.
- (6) Lambe, F.; Ochieng, C. *Improved Cookstoves in Central America: Health Impacts and Uptake*; Stockholm Environment Institute, 2015.
- (7) DANE. Encuesta nacional de calidad de vida (ECV). 2018, <https://www.dane.gov.co/index.php/estadisticas-por-tema/salud/calidad-de-vida-ecv/encuesta-nacional-de-calidad-de-vida-ecv-2018> (accessed Sept 30, 2019).
- (8) Pérez Bayer, J.; Graciano Bustamante, D.; Gómez Betancur, J. Caracterización Energética y Emisiones de Una Estufa de Cocción Ecoeficiente Con Biomasa a Diferentes Altitudes. *Ing. Mecánica* **2013**, *16*, 227–237.
- (9) Jetter, J.; Zhao, Y.; Smith, K. R.; Khan, B.; Yelverton, T.; Decarlo, P.; Hays, M. D. Pollutant Emissions and Energy Efficiency under Controlled Conditions for Household Biomass Cookstoves and Implications for Metrics Useful in Setting International Test Standards. *Environ. Sci. Technol.* **2012**, *46*, 10827–10834.
- (10) Instituto Nacional de Salud. Carga de Enfermedad Ambiental en Colombia. <https://www.ins.gov.co/Direcciones/ONS/Informes/10%20Carga%20de%20enfermedad%20ambiental%20en%20Colombia.pdf> (accessed Sep 30, 2019).
- (11) Ministerio de Minas y Energías. *Programa de Uso Racional y Eficiente de Energía y Fuentes No Convencionales—PROURE*: República de Colombia, Bogotá, D.C. Colombia, 2010.
- (12) Consorcio Estrategia Rural Sostenible; Unidad de Planeación Minero Energética UPME; Ministerio de Minas y Energías. *Realizar Un Estudio Que Permita Formular Un Programa Actualizado de Sustitución Progresiva de Leña Como Energético En El Sector Residencial En Colombia*: Bogotá, D.C. Colombia, 2019.
- (13) Sánchez-Triana, E.; Ahmed, K.; Yewande, A. *Prioridades Ambientales Para La Reducción de La Pobreza En Colombia: Un Análisis Ambiental Del País Para Colombia*; Banco Mundial, 2007.
- (14) Ministerio de Ambiente y Desarrollo Sostenible. *Lineamientos Para Un Programa Nacional de Estufas Eficientes Para Cocción Con Leña*; República de Colombia, 2015.
- (15) Fundación Natura. *Estufas Eficientes de Leña Como Contribución a La Calidad de Vida, Al Uso Eficiente de La Energía y La Reducción de Emisiones de GEI En Areas Rurales de Antioquia y Santander, Colombia: Documento de Sistematización y Suplemento Técnico*: Bogotá, D.C. Colombia, 2015; p 130.
- (16) MinAmbiente. *Informe de Gestión Ministerio de Ambiente y Desarrollo Sostenible 2019*: Bogotá, D.C. Colombia, 2019.
- (17) Obi, O. F.; Ezeoha, S. L.; Okorie, I. C. Energetic Performance of a Top-Lit Updraft (TLUD) Cookstove. *Renewable Energy* **2016**, *99*, 730–737.
- (18) Varunkumar, S. *Packed Bed Gasification-Combustion in Biomass Based Domestic Stoves and Combustion Systems*; Indian Institute of Science, 2014.
- (19) Pérez, J. F.; Benjumea, P. N.; Melgar, A. Sensitivity Analysis of a Biomass Gasification Model in Fixed Bed Downdraft Reactors: Effect of Model and Process Parameters on Reaction Front. *Biomass Bioenergy* **2015**, *83*, 403–421.
- (20) Agudelo, A. F.; Lenis-Rodas, Y. A.; Pérez, J. F. Analysis of Statistical Repeatability of a Fixed Bed Downdraft Biomass Gasification Facility. *Appl. Therm. Eng.* **2013**, *51*, 1006–1016.
- (21) Carvalho, R. L.; Jensen, O. M.; Tarelho, L. A. C. Mapping the Performance of Wood-Burning Stoves by Installations Worldwide. *Energy Build.* **2016**, *127*, 658–679.
- (22) Carter, E. M.; Shan, M.; Yang, X.; Li, J.; Baumgartner, J. Pollutant Emissions and Energy Efficiency of Chinese Gasifier Cooking Stoves and Implications for Future Intervention Studies. *Environ. Sci. Technol.* **2014**, *48*, 6461–6467.
- (23) Nižetić, S.; Papadopoulos, A.; Radica, G.; Zanki, V.; Artçı, M. Using Pellet Fuels for Residential Heating: A Field Study on Its Efficiency and the Users' Satisfaction. *Energy Build.* **2019**, *184*, 193–204.
- (24) Chen, Y.; Shen, G.; Su, S.; Du, W.; Huangfu, Y.; Liu, G.; Wang, X.; Xing, B.; Smith, K. R.; Tao, S. Efficiencies and Pollutant Emissions from Forced-Draft Biomass-Pellet Semi-Gasifier Stoves: Comparison of International and Chinese Water Boiling Test Protocols. *Energy Sustainable Dev.* **2016**, *32*, 22–30.
- (25) Arora, P.; Jain, S.; Sachdeva, K. ScienceDirect Laboratory Based Assessment of Cookstove Performance Using Energy and Emission Parameters for North Indian Cooking Cycle. *Biomass Bioenergy* **2014**, *69*, 211–221.
- (26) Sonarkar, P. R.; Chaurasia, A. S. Thermal Performance of Three Improved Biomass-fired Cookstoves Using Fuel Wood, Wood Pellets and Coconut Shell. *Environ. Dev. Sustain.* **2018**, *21*, 1429–1449.
- (27) Du, W.; Shen, G.; Chen, Y.; Zhu, X.; Zhuo, S.; Zhong, Q.; Qi, M.; Xue, C.; Liu, G.; Zeng, E.; Xing, B.; Tao, S. Comparison of Air Pollutant Emissions and Household Air Quality in Rural Homes Using Improved Wood and Coal Stoves. *Atmos. Environ.* **2017**, *166*, 215–223.
- (28) Global Alliance for Clean Cooks Stoves. The Water Boiling Test, Version 4.2.3, [www.cleancookstoves.org/binary-data/DOCUMENT/file/000/000/399-1.pdf](http://www.cleancookstoves.org/binary-data/DOCUMENT/file/000/000/399-1.pdf) (accessed Oct 5, 2019).
- (29) MacCarty, N.; Still, D.; Ogle, D. Fuel Use and Emissions Performance of Fifty Cooking Stoves in the Laboratory and Related Benchmarks of Performance. *Energy Sustainable Dev.* **2010**, *14*, 161–171.
- (30) Suresh, R.; Singh, V. K.; Malik, J. K.; Datta, A.; Pal, R. C. Evaluation of the Performance of Improved Biomass Cooking Stoves with Different Solid Biomass Fuel Types. *Biomass Bioenergy* **2016**, *95*, 27–34.
- (31) Osei, I.; Kemausuor, F.; Commeh, M. K.; Akowuah, J. O.; Owusu-Takyi, L. Design, Fabrication and Evaluation of Non-Continuous Inverted Downdraft Gasifier Stove Utilizing Rice Husk as Feedstock. *Sci. Afr.* **2020**, *8*, No. e00414.
- (32) Tryner, J.; Willson, B. D.; Marchese, A. J. The Effects of Fuel Type and Stove Design on Emissions and Efficiency of Natural-Draft Semi-Gasifier Biomass Cookstoves. *Energy Sustainable Dev.* **2014**, *23*, 99–109.
- (33) Tryner, J.; Tillotson, J. W.; Baumgardner, M. E.; Mohr, J. T.; DeFoort, M. W.; Marchese, A. J. The Effects of Air Flow Rates, Secondary Air Inlet Geometry, Fuel Type, and Operating Mode on the Performance of Gasifier Cookstoves. *Environ. Sci. Technol.* **2016**, *50*, 9754–9763.

- (34) Hanping, C.; Li, B.; Yang, H.; Yang, G.; Zhang, S. Experimental Investigation of Biomass Gasification in a Fluidized Bed Reactor. *Energy Fuels* **2008**, *22*, 3493–3498.
- (35) Bhattacharya, S. C.; Albina, D. O.; Myint Khaing, A. Effects of Selected Parameters on Performance and Emission of Biomass-Fired Cookstoves. *Biomass Bioenergy* **2002**, *23*, 387–395.
- (36) Van Zyl, L.; Tryner, J.; Bilsback, K. R.; Good, N.; Hecobian, A.; Sullivan, A.; Zhou, Y.; Peel, J. L.; Volckens, J. Effects of Fuel Moisture Content on Emissions from a Rocket-Elbow Cookstove. *Environ. Sci. Technol.* **2019**, *53*, 4648–4656.
- (37) Huangfu, Y.; Li, H.; Chen, X.; Xue, C.; Chen, C.; Liu, G. Effects of Moisture Content in Fuel on Thermal Performance and Emission of Biomass Semi-Gasified Cookstove. *Energy Sustainable Dev.* **2014**, *21*, 60–65.
- (38) Reed, T. B.; Larson, R. A Wood-Gas Stove for Developing Countries. *Energy Sustainable Dev.* **1996**, *3*, 34–37.
- (39) Varunkumar, S.; Rajan, N. K. S.; Mukunda, H. S. Experimental and Computational Studies on a Gasifier Based Stove. *Energy Convers. Manage.* **2012**, *53*, 135–141.
- (40) Mehta, Y.; Richards, C. Effect of Air Flow Rate and Secondary Air Jets on the Operation of TLUD Gasifier Cookstove. *Int. J. Sustain. Energy* **2020**, *39*, 207–217.
- (41) Champion, W. M.; Grieshop, A. P. Pellet-Fed Gasifier Stoves Approach Gas-Stove like Performance during in-Home Use in Rwanda. *Environ. Sci. Technol.* **2019**, *53*, 6570–6579.
- (42) Deng, M.; Zhang, S.; Shan, M.; Li, J.; Baumgartner, J.; Carter, E.; Yang, X. The Impact of Cookstove Operation on PM<sub>2.5</sub> and CO Emissions: A Comparison of Laboratory and Field Measurements. *Environ. Pollut.* **2018**, *243*, 1087–1095.
- (43) Jetter, J. J.; Kariher, P. Solid-Fuel Household Cook Stoves: Characterization of Performance and Emissions. *Biomass Bioenergy* **2009**, *33*, 294–305.
- (44) Raman, P.; Ram, N. K.; Murali, J. Improved Test Method for Evaluation of Bio-Mass Cook-Stoves. *Energy* **2014**, *71*, 479–495.
- (45) Arora, P.; Sharma, D.; Kumar, P.; Jain, S. Assessment of Clean Cooking Technologies under Different Fuel Use Conditions in Rural Areas of Northern India. *Chemosphere* **2020**, *257*, 127315.
- (46) Gupta, A.; Mulukutla, A. N. V.; Gautam, S.; TaneKhan, W.; Waghmare, S. S.; Labhasetwar, N. K. Development of a Practical Evaluation Approach of a Typical Biomass Cookstove. *Environ. Technol. Innovation* **2020**, *17*, 100613.
- (47) Kshirsagar, M. P.; Kalamkar, V. R. Application of Multi-Response Robust Parameter Design for Performance Optimization of a Hybrid Draft Biomass Cook Stove. *Renewable Energy* **2020**, *153*, 1127–1139.
- (48) Kirch, T.; Medwell, P. R.; Birzer, C. H. Natural Draft and Forced Primary Air Combustion Properties of a Top-Lit up-Draft Research Furnace. *Biomass Bioenergy* **2016**, *91*, 108–115.
- (49) Roden, C. A.; Bond, T. C.; Conway, S.; Osorto Pinel, A. B.; MacCarty, N.; Still, D. Laboratory and Field Investigations of Particulate and Carbon Monoxide Emissions from Traditional and Improved Cookstoves. *Atmos. Environ.* **2009**, *43*, 1170–1181.
- (50) Klauser, F.; Carlon, E.; Kistler, M.; Schmidl, C.; Schwabl, M.; Sturmlechner, R.; Haslinger, W.; Kasper-Giebl, A. Emission Characterization of Modern Wood Stoves under Real-Life Oriented Operating Conditions. *Atmos. Environ.* **2018**, *192*, 257–266.
- (51) Kaur-Sidhu, M.; Ravindra, K.; Mor, S.; John, S. Emission Factors and Global Warming Potential of Various Solid Biomass Fuel-Cook Stove Combinations. *Atmos. Pollut. Res.* **2020**, *11*, 252–260.
- (52) Caubel, J. J.; Rapp, V. H.; Chen, S. S.; Gadgil, A. J. Practical Design Considerations for Secondary Air Injection in Wood-Burning Cookstoves: An Experimental Study. *Dev. Eng.* **2020**, *5*, 100049.
- (53) González, W. A.; Pérez, J. F. CFD Analysis and Characterization of Biochar Produced via Fixed-Bed Gasification of Fallen Leaf Pellets. *Energy* **2019**, *186*, 115904.
- (54) Champion, W. M.; Warren, S. H.; Kooter, I. M.; Preston, W.; Krantz, Q. T.; DeMarini, D. M.; Jetter, J. J. Mutagenicity- and Pollutant-Emission Factors of Pellet-Fueled Gasifier Cookstoves: Comparison with Other Combustion Sources. *Sci. Total Environ.* **2020**, *739*, 139488.
- (55) Kirch, T.; Medwell, P. R.; Birzer, C. H.; van Eyk, P. J. Small-Scale Autothermal Thermochemical Conversion of Multiple Solid Biomass Feedstock. *Renewable Energy* **2020**, *149*, 1261–1270.
- (56) González, W. A.; Pérez, J. F.; Chapela, S.; Porteiro, J. Numerical Analysis of Wood Biomass Packing Factor in a Fixed-Bed Gasification Process. *Renewable Energy* **2018**, *121*, 579–589.
- (57) Chica, E.; Pérez, J. F. Development and Performance Evaluation of an Improved Biomass Cookstove for Isolated Communities from Developing Countries. *Case Stud. Therm. Eng.* **2019**, *14*, 100435.
- (58) Ismail, O.; Urbanus, M.; Murage, H.; Francis, O. Conversion of Rice Husks into an Energy Source through Gasification Technology. *Int. J. Sci. Res.* **2016**, *5*, 1264–1268.
- (59) United Nations Foundation. Clean Cook Catalog. <http://catalog.cleancookstoves.org/pages/about> (accessed Oct 1, 2020).
- (60) Fedak, K. M.; Good, N.; Dahlke, J.; Hecobian, A.; Sullivan, A.; Zhou, Y.; Peel, J. L.; Volckens, J. Chemical Composition and Emissions Factors for Cookstove Startup (Ignition) Materials. *Environ. Sci. Technol.* **2018**, *52*, 9505–9513.
- (61) Torres-Rojas, D.; Deng, L.; Shannon, L.; Fisher, E. M.; Joseph, S.; Lehmann, J. Carbon and Nitrogen Emissions Rates and Heat Transfer of an Indirect Pyrolysis Biomass Cookstove. *Biomass Bioenergy* **2019**, *127*, 105279.
- (62) Caubel, J. J.; Rapp, V. H.; Chen, S. S.; Gadgil, A. J. Optimization of Secondary Air Injection in a Wood-Burning Cookstove: An Experimental Study. *Environ. Sci. Technol.* **2018**, *52*, 4449–4456.
- (63) Valencia-López, A. M.; Bustamante, F.; Loukou, A.; Stelzner, B.; Trimis, D.; Frenklach, M.; Slavinskaya, N. A. Effect of Benzene Doping on Soot Precursors Formation in Non-Premixed Flames of Producer Gas (PG). *Combust. Flame* **2019**, *207*, 265–280.
- (64) Mitchell, E. J. S.; Ting, Y.; Allan, J.; Lea-Langton, A. R.; Spracklen, D. V.; McFiggans, G.; Coe, H.; Routledge, M. N.; Williams, A.; Jones, J. M. Pollutant Emissions from Improved Cookstoves of the Type Used in Sub-Saharan Africa. *Combust. Sci. Technol.* **2020**, *192*, 1582–1602.
- (65) Mott, R. L. *Applied Fluid Mechanics*, 4th ed.; Prentice Hall Career & Technology, 1994.
- (66) Sukhwani, V. K.; Patidar, N.; Nagar Govt, A. Design and Performance Evaluation of Improved Biogas Stove (IBS) by Preheating of Biogas. *Int. J. Sci. Eng. Technol.* **2017**, *6*, 70–74.
- (67) Demissie, S. W.; Ramayya, V. A.; Nega, D. T. Design, Fabrication and Testing of Biogas Stove for “Areke” Distillation: The Case of Arsi Negele, Ethiopia, Targeting Reduction of Fuel-Wood Dependence. *Int. J. Eng. Res. Technol.* **2016**, *5*, 354.
- (68) Orhororo, E. K.; Oyejide, J. .; Abubakar, S. A. Design and Construction of an Improved Biogas Stove. *J. Environ. Eng. Technol.* **2018**, *14*, 325–335.
- (69) Petro, L. M.; Machunda, R.; Tumbo, S.; Kivevele, T. Theoretical and Experimental Performance Analysis of a Novel Domestic Biogas Burner. *J. Energy* **2020**, *2020*, 1–9.
- (70) Lenis, Y. A.; Pérez, J. F. Gasification of Sawdust and Wood Chips in a Fixed Bed under Autothermal and Stable Conditions. *Energy Sources, Part A* **2014**, *36*, 2555–2565.
- (71) Lenis, Y. A.; Pérez, J. F.; Melgar, A. Fixed Bed Gasification of Jacaranda Copaia Wood: Effect of Packing Factor and Oxygen Enriched Air. *Ind. Crops Prod.* **2016**, *84*, 166–175.
- (72) Campoy, M.; Gómez-Barea, A.; Vidal, F. B.; Ollero, P. Air-Steam Gasification of Biomass in a Fluidised Bed: Process Optimisation by Enriched Air. *Fuel Process. Technol.* **2009**, *90*, 677–685.
- (73) Erlich, C.; Fransson, T. H. Downdraft Gasification of Pellets Made of Wood, Palm-Oil Residues Respective Bagasse: Experimental Study. *Appl. Energy* **2011**, *88*, 899–908.
- (74) Diez, H. E.; Gómez, I. N.; Pérez, J. F. Mass, Energy, and Exergy Analysis of the Microgasification Process in a Top-Lit Updraft

Reactor: Effects of Firewood Type and Forced Primary Airflow. *Sustain. Energy Technol. Assessments* **2018**, *29*, 82–91.

(75) Sohi, S. P.; Krull, E.; Lopez-Capel, E.; Bol, R. A Review of Biochar and Its Use and Function in Soil. *Adv. Agron.* **2010**, *105*, 47–82.

(76) Gutiérrez, J.; Rubio-Clemente, A.; Pérez, J. F. Effect of Main Solid Biomass Commodities of Patula Pine on Biochar Properties Produced under Gasification Conditions. *Ind. Crops Prod.* **2021**, *160*, 113123.

(77) Pérez, J. F.; Pelaez-Samaniego, M. R.; Garcia-Perez, M. Torrefaction of Fast-Growing Colombian Wood Species. *Waste Biomass Valorization* **2019**, *10*, 1655–1667.

(78) Benedetti, V.; Patuzzi, F.; Baratieri, M. Characterization of Char from Biomass Gasification and Its Similarities with Activated Carbon in Adsorption Applications. *Appl. Energy* **2018**, *227*, 92–99.

(79) Hubbard, W. G. Wood Bioenergy. *Bioenergy* **2015**, 55–71.

(80) Whittaker, C.; Shield, I. Short Rotation Woody Energy Crop Supply Chains. *Bioenergy Biorefining* **2016**, 217–248.

(81) Pérez, J. F.; Melgar, A.; Benjumea, P. N. Effect of Operating and Design Parameters on the Gasification/Combustion Process of Waste Biomass in Fixed Bed Downdraft Reactors: An Experimental Study. *Fuel* **2012**, *96*, 487–496.

(82) American Conference of Governmental Industrial Hygienists. *Industrial Ventilation: A Manual of Recommended Practice for Design*, 23rd ed.; American Conference of Governmental Industrial Hygienists: Cincinnati, Ohio, 1997; Vol. 552.

(83) Saud, T.; Mandal, T. K.; Gadi, R.; Singh, D. P.; Sharma, S. K.; Saxena, M.; Mukherjee, A. Emission Estimates of Particulate Matter (PM) and Trace Gases (SO<sub>2</sub>, NO and NO<sub>2</sub>) from Biomass Fuels Used in Rural Sector of Indo-Gangetic Plain, India. *Atmos. Environ.* **2011**, *45*, 5913–5923.

(84) U.S. Environmental Protection Agency; Partnership for Clean Indoor Air. *The Water Boiling Test, Version 4.2.3, Cook Stove Emissions and Efficiency in a Controlled Laboratory Setting*, 2014; Vol. 2.

(85) Arora, P.; Das, P.; Jain, S.; Kishore, V. V. N. A Laboratory Based Comparative Study of Indian Biomass Cookstove Testing Protocol and Water Boiling Test. *Energy Sustainable Dev.* **2014**, *21*, 81–88.

(86) Guo, F.; Dong, Y.; Dong, L.; Guo, C. Effect of Design and Operating Parameters on the Gasification Process of Biomass in a Downdraft Fixed Bed: An Experimental Study. *Int. J. Hydrogen Energy* **2014**, *39*, 5625–5633.

(87) Llamosa, E.; Botero, M. Promedios y Rangos Para El Aseguramiento de La Calidad de Los Resultados de Calibración de Acuerdo Con La Norma Técnica NTC- ISO/IEC 17025. *Sci. Tech.* **2007**, *35*, 455–460.

(88) Montgomery, D. C. *Design and Analysis of Experiments*, 2nd ed.; Grupo Noriega Editores, Ed.; LIMUSA, S.A: Arizona, 2004.